HHS Public Access

Author manuscript

Cell Rep. Author manuscript; available in PMC 2019 November 22.

Published in final edited form as:

Cell Rep. 2019 September 17; 28(12): 3092–3104.e5. doi:10.1016/j.celrep.2019.08.038.

Robust Iterative Stimulation with Self-Antigens Overcomes CD8+ T Cell Tolerance to Self- and Tumor Antigens

Christine E. Nelson[1,2], **Emily A. Thompson**[1,2], **Clare F. Quarnstrom**[1,2], **Kathryn A. Fraser**[1,2], **Davis M. Seelig**[3], **Siddheshvar Bhela**[1,2], **Brandon J. Burbach**[1,4], **David Masopust**[1,2], **Vaiva Vezys**[1,2,5,*]

[1]Center for Immunology, University of Minnesota, Minneapolis, MN 55455, USA

[2]Department of Microbiology and Immunology, University of Minnesota, Minneapolis, MN 55455, USA

[3]Department of Veterinary Clinical Sciences, University of Minnesota, St. Paul, MN 55118, USA

[4]Department of Laboratory Medicine and Pathology, University of Minnesota, Minneapolis, MN 55455, USA

[5]Lead Contact

SUMMARY

The immune system adapts to constitutive antigens to preserve self-tolerance, which is a major barrier for anti-tumor immunity. Antigen-specific reversal of tolerance constitutes a major goal to spur therapeutic applications. Here, we show that robust, iterative, systemic stimulation targeting tissue-specific antigens in the context of acute infections reverses established $CD8^+$ T cell tolerance to self, including in T cells that survive negative selection. This strategy results in large numbers of circulating and resident memory self-specific $CD8^+$ T cells that are widely distributed and can be co-opted to control established malignancies bearing self-antigen without concomitant autoimmunity. Targeted expansion of both self- and tumor neoantigen-specific T cells acts synergistically to boost anti-tumor immunity and elicits protection against aggressive melanoma. Our findings demonstrate that T cell tolerance can be re-adapted to responsiveness through robust antigenic exposure, generating self-specific $CD8^+$ T cells that can be used for cancer treatment.

Graphical Abstract

*Correspondence: vvezys@umn.edu.

AUTHOR CONTRIBUTIONS

Conceptualization, C.E.N. and V.V.; Methodology, C.E.N., E.A.T., C.F.Q., B.J.B., D.M., and V.V.; Validation, C.E.N., E.A.T., C.F.Q., and S.B.; Formal Analysis, C.E.N., E.A.T., C.F.Q., D.M.S., and S.B.; Investigation, C.E.N., E.A.T., C.F.Q., D.M.S., S.B., and K.A.F.; Resources, D.M. and V.V.; Writing – Original Draft, C.E.N. and V.V.; Writing – Review & Editing, C.E.N., E.A.T., C.F.Q., K.A.F., B.J.B., and V.V.; Visualization, C.E.N., E.A.T., C.F.Q., D.M.S., and S.B.; Supervision & Project Administration, V.V.; Funding Acquisition, C.E.N., E.A.T., and V.V.

SUPPLEMENTAL INFORMATION

Supplemental Information can be found online at https://doi.org/10.1016/j.celrep.2019.08.038.

DECLARATIONS OF INTERESTS

The authors declare no competing interests.

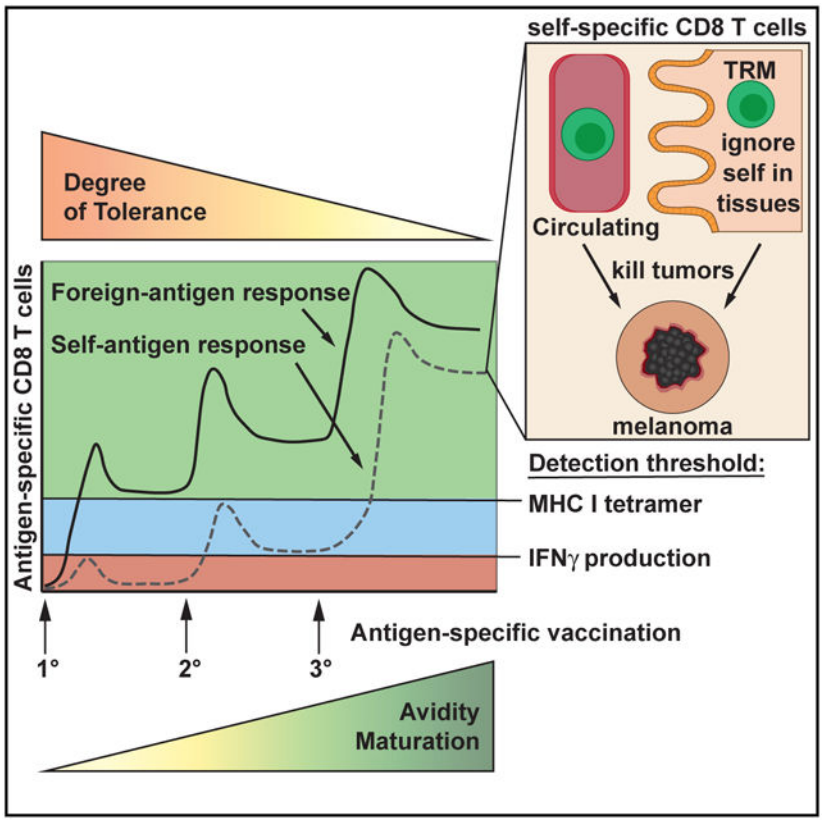

In Brief

Nelson et al. show that immune tolerance to self is not a fixed state and can be overcome with robust, iterative stimulation in the context of infection. Autoreactive $CD8^+$ T cells expanded with this method can be co-opted to target tumors bearing shared self-antigen without associated autoimmunity.

INTRODUCTION

The random rearrangement of T cell receptor (TCR) genes generates T cells with a broad range of specificities, including T cells specific for self-antigens. To circumvent this, self-specific T cells escaping central tolerance acclimate to self-antigen and become non-responsive (Mueller, 2010; Sebzda et al., 1994). While tolerance is ideal for controlling autoimmunity, it is a barrier for tumor immunotherapy, as many of the same tolerance mechanisms restrain tumor-specific T cells (Schietinger et al., 2016).

Tumor neo-antigens are important targets for immunotherapies (Larkin et al., 2015; Schumacher and Schreiber, 2015). However, targeting neo-antigens is complex, as they are unique and unevenly expressed. Self-antigens can be uniformly overexpressed in tumors. Self-specific CD8 T cells also have the potential to patrol for cancer recurrence, whereas neo-antigen-specific T cells could lose this ability, as relapses may not harbor the same neo-antigens (McGranahan and Swanton, 2017). Thus, many groups have attempted to generate populations of self-specific T cells as immunotherapies (Malik et al., 2017; Overwijk et al.,

1998, 1999; Xiang et al., 2017). However, such manipulation may precipitate autoimmunity. Thus, there is an opportunity for the development of *in vivo* modalities that activate tolerant T cells in a targeted fashion to generate large numbers of self-specific T cells for immunotherapy, yet induce no or self-resolving autoimmune pathology.

Tissue resident memory T cells (T_{RM}) play a significant role in anti-tumor immunity (Enamorado et al., 2017; Malik et al., 2017; Nizard et al., 2017). Recently, it has been shown that both circulating and T_{RM} cells have anti-tumor potential and may synergize to prevent tumor outgrowth (Enamorado et al., 2017). Thus, simultaneously enhancing both T cell populations is key for optimal anti-tumor responsiveness (Boddupalli et al., 2016; Nizard et al., 2017).

We set out to probe the plasticity of self-specific CD8 T cells under the control of central and/or peripheral tolerance. Through robust systemic and iterative stimulation with vectors containing self-antigens, functional self-specific CD8 T cells can be generated from the previously non-responsive CD8 T cell repertoire. This is true for endogenous self-specific CD8 T cells and high-affinity transgenic self-specific CD8 T cells. Cumulative antigenic stimulation drives avidity maturation of tolerant CD8 T cells and contributes to increased antigen sensing. Expanded self-specific CD8 T cells are dispersed throughout the body and become T_{RM} in lymphoid and non-lymphoid organs. The amplification of these self-specific T cells delays the growth of tumors bearing self-antigens without autoimmunity. Immunotherapy using neo-antigen-specific CD8 T cells is augmented by self-specific CD8 T cell responses. These studies reveal that antigen-induced T cell non-responsiveness can be reversed with proper antigenic exposure and opens the possibility of co-opting self-specific T cell responses for the treatment of cancer.

RESULTS

Reversal of Established Peripheral Tolerance in High-Affinity Self-Specific CD8 T Cells

We used intestinal fatty acid-binding protein (iFABP)-Ova mice, in which ovalbumin (Ova) is a self-protein in the small intestine, to generate a known population of anergic CD8 T cells (Pauken et al., 2015; Vezys et al., 2000). When naive OTI (high-affinity transgenic CD8 T cells specific for Ova) are transferred to adult iFABP-Ova mice, OTI cells quickly become tolerized in the absence of infection, antigen-presenting cell (APC) maturation signals, or checkpoint blockade (Nelson et al., 2019; Pauken et al., 2015; Vezys and Lefrançois, 2002; Vezys et al., 2000). After 30 days in iFABP-Ova hosts, OTI cells are PD-1^+, do not produce cytokines, and are refractory to PD-L1, PD-1, CTLA4, LAG-3, and/or TIM-3 blockade (Nelson et al., 2019; Pauken et al., 2015). These data mirror the dysfunction of tumor-specific CD8 T cells, which is thought to be fixed by day 14 after initial antigen encounter (Philip et al., 2017; Schietinger et al., 2012., 2016). Dysfunctional self-specific OTI cells are maintained long term (at least 359 days) in iFABP-Ova mice (Figures 1A, 1B, and S1).

To assess whether non-responsiveness could be reversed for high-affinity OTI cells, iFABP-Ova mice with tolerant OTI cells were infected with vesicular stomatitis virus (VSV)-Ova. This induced OTI expansion in the blood and non-lymphoid tissues (NLTs), despite our

previous data that tolerant OTI cells do not proliferate or produce cytokines after checkpoint blockade alone (Figures 1B, 1C, and S1) (Nelson et al., 2019; Pauken et al., 2015). A 53-fold expansion in peripheral blood leukocytes (PBLs) occurred by day 7 after VSV-Ova and these cells are maintained long term (Figures 1C and S1). Thus, tolerance can be reversed *in vivo* for high-affinity self-specific CD8 T cell populations that appear to be in a fixed dysfunctional state and are resistant to checkpoint blockade.

Tolerance reversal has been shown to be transient, and self-specific T cell populations return to a tolerant state (Schietinger et al., 2012). We tested whether additional antigenic stimulation could continue to expand OTI cells. Secondary infection (2°) with *Listeria monocytogenes*-Ova (LM-Ova) and tertiary infection (3°) with vaccinia virus-Ova (VV-Ova) yielded an ~700-fold expansion of OTI in iFABP-Ova mice by day 7 after the last infection, compared to the starting, tolerant OTI population (Figure 1C). OTI numbers increased in the spleen, mesenteric lymph node (mLN), and small intestinal intraepithelial lymphocytes (IELs) (Figure 1D). Not only was proliferation of OTI cells induced but interferon γ (IFN-γ) and tumor necrosis factor α (TNF-α) production was also restored (Figures 1A, 1E, and S2) (Nelson et al., 2019; Pauken et al., 2015). Therefore, dysfunction is reversible for high-affinity tolerant CD8 T cells through antigen-driven signals, and the resulting population is functional and can continue to be expanded.

Self-Specific T Cell Expansion Results in Avidity Maturation but Not Sustained Autoimmunity

To determine whether intestinal autoimmunity was induced after tolerance reversal in OTI cells, weight loss was measured in iFABP-Ova mice (Vezys et al., 2000). All of the mice maintained or gained weight after 3° infection (Figure 1F). Serum iFABP concentration is used both in animal models and in the clinic to indicate small intestinal damage (Derikx et al., 2009). We found a basal level of serum iFABP in iFABP-Ova mice with anergic OTI (tolerant OTI versus no OTI) (Figure S2). At day 0 of 3° infection, there is little iFABP in the serum, indicating no ongoing autoimmunity (3° day 0). By day 10 after 3° infection, serum iFABP was increased, despite little weight loss. This was a transient increase in serum iFABP, as levels were back to baseline by day 30 after 3° (Figure S2). This is similar to previously published results indicating that self-reactive CD8 T cells do not necessarily induce pathology in antigen-bearing non-malignant tissue after tolerance reversal (Nelson et al., 2019). Ultimately, strong antigenic stimulation can induce the expansion of high-affinity self-specific CD8 T cells, resulting in tissue migration and induction of effector functions.

Avidity maturation has been shown to be critical for the expansion of self-specific T cells (Amrani et al., 2000; Xiang et al., 2017). Tolerance reversal of OTI cells was correlated with increased K^b-SIINFEKL tetramer geometric mean fluorescence intensity (GMFI) after each infection (Figures 1G and 1H). This indicated that TCR levels and antigen sensitivity is enhanced with each stimulation. TCR avidity was correlated with increased PD-1 expression (Figure 1I). This is reminiscent of avidity maturation that occurs in self-specific CD8 T cells as they participate in autoimmune diabetic pathology or tumor control (Amrani et al., 2000; Xiang et al., 2017). Thus, increased antigen sensitivity is a characteristic of T cells undergoing tolerance reversal.

Incomplete Negative Selection of Endogenous Self-Specific CD8 T Cells

We showed that established peripheral CD8 T cell tolerance can be overcome with iterative stimulation in iFABP-Ova mice. We then tested whether the same would be true for endogenous self-specific CD8 T cells. In iFABP-Ova mice, Ova is expressed via AIRE and K^b-SIINFEKL-specific CD8 T cells are subject to both central and peripheral tolerance (Lee et al., 2007; Vezys et al., 2000). Endogenous K^b-SIINFEKL-specific CD8 T cell responses are not observed after infection with single Ova-bearing vectors, indicating that either negative selection is robust or T cell tolerance is established (Figure 2A). However, low-affinity self-specific T cells can escape negative selection (Enouz et al., 2012; Zehn and Bevan, 2006). As sequential infections were effective at generating ex-tolerant OTI, we hypothesized that one round of vaccination was insufficient to break tolerance for endogenous self-specific CD8 T cells. This is in line with studies showing that two rounds of vaccination were required to precipitate CD8 T cell-mediated diabetes, although these T cells could not be detected with major histocompatibility complex class I (MHC I) tetramers (Enouz et al., 2012). When LM-Ova was given as a 2° to iFABP-Ova mice, very few self-specific CD8 T cells were detected (Figure 2B). However, when 3° with VV-Ova was given, a significant population of self-specific CD8 T cells arose (Figure 2C). This population was below the level of detection when VV-Ova was given alone as an initial infection (1°) (Figure 2A). By day 30 after 3°, the K^b-SIINFEKL self-specific CD8 T cells accounted for as much as 60% of total CD8 T cells in self-antigen-bearing mice (Figure 2D). We noted greater variability in the K^b-SIINFEKL-specific CD8 T cell burst size in iFABP-Ova versus C57BL/6 mice (Figure 2D). This is likely due to the numerical variance of K^b-SIINFEKL-specific CD8 T cell precursors in iFABP-Ova mice, a result of negative selection. The expansion of self-specific CD8 T cells was not an artifact of priming recent thymic emigrants, as similar T cell responses were observed in mice that were thymectomized before 1 ° vaccination (Figure 2E). These data indicate that negative selection is incomplete, and despite tolerance mechanisms, a population of self-specific CD8 T cells exists within the endogenous repertoire that can be expanded.

Robust Stimulation of Self-Specific CD8 T Cells Induces Functional Changes

We interrogated the functional and phenotypic characteristics of K^b-SIINFEKL-specific CD8 T cells expanded under self- and non-self-conditions. The expressions of PD-1 and granzyme B by K^b-SIINFEKL-specific CD8 T cells in iFABP-Ova and C57BL/6 are not significantly different (Figure 3A). The PD-1^{lo} phenotype was expected in C57BL/6 animals, as the vectors are short-lived and antigen is quickly cleared. However, PD-1^{lo} expression was unexpected in iFABP-Ova mice, as Ova self-antigen is persistently presented on MHC I (Lee et al., 2007; Nelson et al., 2019; Pauken et al., 2015; Vezys and Lefrançois, 2002; Vezys et al., 2000). The PD-1^{lo} phenotype on endogenous K^b-SIINFEKL-specific CD8 T cells is likely due to low TCR affinity and suboptimal signaling to induce PD-1 (Jiang et al., 2016). The self-specific CD8 T cell population has a lower GMFI of Kb-SIINFEKL tetramer binding compared to the non-self-population, indicating lower TCR affinity (Figure 3B). MHC tetramers for vector epitopes (N and B8R) show similar GMFIs between C57BL/6 and iFABP-Ova (Figure 3B). After iterative immunizations, K^b-SIINFEKL CD8 T cells in iFABP-Ova mice produced cytokines upon peptide stimulation and had cytotoxic function *in vivo* (Figures 3C and 3D). Despite reactivity to self-antigen by

functional assays, autoimmunity was not observed in the small intestine (Figure S3B) (Nelson et al., 2019; Vezys and Lefrançois, 2002). Ultimately, self-specific CD8 T cells are functional relative to population expansion size and are not necessarily pathogenic (Figures 3A–3D and S3).

Tolerance Reversal Is Coupled to Antigen-Driven Avidity Maturation

It was striking that the expansion of self-specific CD8 T cells after 3° was greater than 1° responses in C57BL/6 mice (Figures 2D and 2E). We hypothesized that K^b-SIINFEKL-specific CD8 T cells were present and responsive before 3° immunization in iFABP-Ova mice, despite a lack of detection via MHCI tetramers (Figure 2) Hernández et al., 2000). We examined the self-specific responses in iFABP-Ova mice after 1° and 2° using cytokine production as a readout after *ex vivo* peptide stimulation. With this method, K^b-SIINFEKL-specific CD8 T cells were readily visualized after 2° in iFABP-Ova mice, despite being very rare via MHC I tetramer staining (Figures 2B and 3C). We found that the number of K^b-SIINFEKL-specific CD8 T cells differed significantly between the two detection methods (Figure 3E). The number of T cells detected via cytokine production in iFABP-Ova animals at 2° was equivalent to the number of MHC I tetramer-binding cells in C57BL/6 animals after 1° (Figures 3E and 3F). Therefore, the lack of MHC I tetramer-binding cells at 2° was not due to low numbers, as tetramers easily detected equivalent numbers of non-self-specific CD8 T cells (Figures 3E and 3F, dotted line). When the number of self-specific CD8 T cells at 2° was normalized to the number of cytokine producers in B6 1° mice, the same trend was observed (Figure S3C). Thus, low-affinity self-specific CD8 T cells are underrepresented by MHC I tetramers before 3° immunization.

We hypothesized that multiple immunizations enhanced MHC I tetramer binding and increased functional avidity. To test this, we evaluated functionality in a peptide dose-response curve before and after 3°. Before 3°, cytokine production was suboptimal in self-specific CD8 T cells, as compared to non-self-specific T cells (Figures 3G and S3A). However, after 3°, self-specific T cells produced significantly more IFN-γ than at 2°. When the *in vivo* killing capacity was normalized to antigen-specific T cell numbers, this function increased from 1° to 3° (Figure S3B). This demonstrates a greater sensitivity to antigen for endogenous self-specific CD8 T cells after 3° vaccination, establishing avidity maturation as a corollary of iterative stimulation.

Repeated Stimulation Induces Cell-Intrinsic Changes in Self-Specific CD8 T Cells with Memory T Cell Characteristics

Self-specific T cells can be rendered non-responsive through both cell-intrinsic and cell-extrinsic factors (Mueller, 2010). To determine whether tolerance reversal is a result of environmental or T cell-intrinsic changes, splenocytes from 2° immunized mice were transferred into antigen-matched naive hosts (Figure 4A). At transfer, very few K^b-SIINFEKL-specific CD8 T cells were detectable via MHC I tetramers in iFABP-Ova mice (Figure 2). Recipient mice were infected with VV-Ova, which alone does not induce MHC I tetramer-binding T cells in iFABP-Ova mice (Figure 2A). After just one infection, iFABP-Ova donor-derived tetramer-binding self-specific CD8 T cells were detectable at high levels

in new hosts (Figure 4A). Thus, tolerance reversal caused by sequential antigenic stimulation leads to cell-intrinsic changes in self-specific CD8 T cells.

Classical memory CD8 T cells do not require continued antigenic stimulation for their survival (Murali-Krishna et al., 1999). However, chronically stimulated T cells become antigen addicted and do not survive in antigen-free hosts (Wherry et al., 2004). To determine whether expanded self-specific CD8 T cells have the characteristics of memory or exhausted cells, we asked whether these T cells could survive long term in an antigen-free host. Equal numbers of boosted K^b-SIINFEKL-specific CD8 T cells were transferred from 3° iFABP-Ova mice to naive C57BL/6 or iFABP-Ova hosts. Similar numbers of donor-derived K^b-SIINFEKL self-specific CD8 T cells were recovered from antigen-free and antigen-bearing hosts 70 days after cell transfer (Figure 4B). Therefore, antigen is not needed to maintain expanded self-specific CD8 T cells, similar to traditional memory CD8 and CD4 T cells (Murali-Krishna et al., 1999; Swain et al., 1999).

Self-specific CD8 T cell activation has been shown to occur via dual TCR expression, in which virus-specific TCRs are activated on T cells also bearing self-reactive TCR (Ji et al., 2010). To test whether this occurred here, we performed dual-MHC I tetramer staining on CD8 T cells in iFABP-Ova animals after 3°. K^b-SIINFEKL-specific CD8 T cells did not bind MHC I tetramers complexed to vaccinia virus (B8R) nor to VSV (N) immunodominant epitopes (Figure 4C). Thus, self-specific T cell response is not attributed to activation through an alternative TCR.

Sequential Infections Are More Robust Than a Persistent Infection at Potentiating Self-Specific CD8 T Cell Responses

We have shown that multiple antigenic encounters are necessary for the expansion of self-specific CD8 T cells. However, persistent infections such as murine cytomegalovirus (MCMV) can also drive large CD8 T cell responses (Snyder et al., 2008). To test whether a persistent infection producing self-antigen could substitute for multiple acute infections, we gave C57BL/6 and iFABP-Ova mice MCMV-Ova. By day 50 post-infection, 0.2% of CD8 T cells were K^b-SIINFEKL specific in iFABP-Ova hosts, and this increased to ~1% by day 150 (Figures 4D and 4E). However, MCMV-Ova infection did not recapitulate the expansion of K^b-SIINFEKL CD8 T cell achieved with 3 rounds of acute infection (~60% of CD8 T cells) (Figure 2D). MCMV-Ova infection did not expand absolute cell numbers, with ~1×10^4 K^b-SIINFEKL-specific CD8 T cells, compared to ~1×10^6 after multiple immunizations (Figures 3D and 4E). Similar numbers of vector (M45)-specific CD8 T cells were detected between groups (Figure 4E). There were significant differences in the IE3-specific CD8 T cells between iFABP-Ova and C57BL/6 mice, suggesting compensation for the blunted K^b-SIINFEKL response in iFABP-Ova animals. Overall, these data demonstrate that sequential immunization is superior to MCMV as a method to expand self-specific CD8 T cells.

Expansion of Melanocyte-Specific Circulating and Resident Memory T Cells

Tolerance to Ova self-antigen is robust in endogenous and adoptive transfer models, but Ova is not a naturally occurring self-antigen. In both mice and humans, the melanocyte protein gp100 is a self-antigen expressed in the skin and is a tumor-associated antigen in melanoma

(Kawakami et al., 1995; Overwijk et al., 1998). Previous studies suggested that melanoma tumor-specific T cell responses can be enhanced via a heterologous prime boost vaccination (Cho et al., 2015; Irvine et al., 1997). We tested whether our sequential immunizations could reverse tolerance for endogenous gp100-specific CD8 T cells in C57BL/6 mice. A single vaccination with VSV-gp100 was insufficient to expand a detectable population of D^b-gp100-specific CD8 T cells (Figure 5A). However, multiple immunizations with gp100-producing vectors expanded a large population of skin-specific CD8 T cells (Figure 5A). The mouse gp100 epitope is thought to have a lower affinity for mouse MHC I than the human gp100 epitope (Overwijk et al., 1998). After 3°, gp100-specific CD8 T cells are functional and equivalently recognize both the mouse and human D^b-gp100 epitopes (Figure S4A–S4C). We observed avidity maturation of the endogenous gp100 antigen-specific T cell pool after boosting, as the GMFIs of tetramer staining increased after 3° (Figure 5B). Multiple gp100-specific CD8 T cell clones responded to immunization; at least seven different Vβ chains were detected in the gp100-specific T cell pool (Figures 5C and S4D). Multiple tolerant T cells are mobilized, and the response is not due to the outgrowth of a single high-affinity clone.

We investigated the NLT distribution of expanded D^b-gp100-specific CD8 T cells. Immunization with gp100 vectors induced widespread dissemination of D^b-gp100-specific CD8 T cells to lymphoid and NLTs, such as the skin, brain, and lung (Figures 5D and 5E). The location of these self-specific T cells in tissue parenchyma versus tissue vasculature was confirmed via intravenous (i.v.) antibody staining (Anderson et al., 2012). The cells in NLT share a common Vβ repertoire, indicating that they originated from common precursors (Figure 5F). The majority of self-specific CD8 T cells in NLTs have a high expression of PD-1, yet many cells in the skin make IFN-γ, albeit to a lower degree compared to secondary lymphoid organ (SLO) cells (Figures 5E, S4E, and S4F). Despite the functionality of gp100-specific CD8 T cells, autoimmune pathology was not observed in the skin (Figure S4G). In all of the model systems investigated, functionality to self-antigens can be observed in boosted CD8 T cell populations without concomitant autoimmunity.

Tissue Residency in Expanded Populations of Self- and Non-self-Specific CD8 T Cells

We showed that expanded self-specific CD8 T cells share some characteristics with non-self-specific memory CD8 T cells. To directly compare boosted self- and non-self-specific CD8 T cells in intact hosts, we used a dual antigen-boosting method. C57BL/6 mice were immunized with both gp100- and Ova-producing vectors simultaneously. Boosted self- and non-self-specific CD8 T cell populations were found in all of the analyzed organs (Figure S5A). The number of self-specific and foreign antigen-specific CD8 T cells were similar in many tissues, such as skin, lung, liver, and mLN, but differed in the salivary gland, female reproductive tract (FRT), brain, spleen, and inguinal LN (iLN). Parabiosis surgery was performed on dual-immunized mice to delineate the number of T_{RM} that are induced after sequential immunization. The majority of D^b-gp100-specific and Ova-specific CD8 T cells found in tissues are T_{RM} (Figure 5G).

Multiple immunizations increased the percent residence, as compared to a 1° response, in tissues such as small intestine, skin, lung, and liver (Figure 5G, striped versus gray bars).

This is also true for mLNs and potentially other SLOs. These data are in line with previously published results indicating that CD8 T cells are resident in many tissues and that anamnestic responses in NLT drive increased T_{RM} deposition in SLO (Beura et al., 2018; Mackay et al., 2013; Sathaliyawala et al., 2013; Steinert et al., 2015; Wakim et al., 2010). Both self- and foreign antigen-specific CD8 T cells fail to conform to the $CD69^{+}CD103^{+}$ phenotype often assigned to T_{RM} (Figure S6) (Mackay et al., 2013; Sathaliyawala et al., 2013). Our data demonstrate the versatility of heterologous prime-boost-boost for the expansion of both self- and foreign antigen-specific CD8 T cells and the potential for inducing large numbers of T_{RM} in SLOs and NLTs.

Expanded Self-Specific CD8 T Cells Control Aggressive Tumor Growth

We next examined whether the expansion of D^{b}-gp100 CD8 T cells could be used to control the growth of melanoma tumors. Mice were challenged with an aggressive mouse-derived B16 melanoma cell line that produces gp100. The amount of gp100 produced in tumors is ~100-fold compared to healthy adjacent skin, which is similar to melanoma in humans (Figure S5H and S5I) (Tjin et al., 2011). The amount of gp100 produced per cell is higher in tumors, likely leading to more MHC-I:gp100 complexes, as compared to healthy skin (Figure S5I). The lack of autoimmunity in boosted mice may be controlled by lower antigen levels in healthy tissue. In naive mice challenged with B16 tumors, 100% of mice develop tumors by day 8 and *de novo* D^{b}-gp100-specific responses are not detected within tumors (Figures 6A and 6B). This is in contrast to B16-Ova tumors, which can induce the activation of K^{b}-SIINFEKL-specific CD8 T cells (Figure 6A). Mice immunized with 1° VSV-gp100 were given 2° vaccination 2 days before B16 challenge and demonstrated delayed tumor incidence, as well as control of tumor growth and size (Figure 6B). The growth delay was accompanied by robust gp100-specific CD8 T cell infiltration into tumors (Figure 6C). Tumor-infiltrating lymphocytes were functional and produced cytokines in response to antigen. Because D^{b}-gp100-specific CD8 T cells were $PD\text{-}1^{hi}$, we tested whether this level of protection could be enhanced by the addition of anti-PD-L1 blockade therapy. However, anti-PD-L1 given at the time of vaccination did not enhance protection from the B16 challenge over 2° vaccination alone (Figures 6D and S5B). Effector self-specific T cells at 2° were sufficient to delay tumor onset, but they were not potentiated by PD-L1 blockade.

We then tested the therapeutic potential of gp100-specific CD8 T cells to delay ongoing tumor growth. B16 cells were injected into naive, 2° Ova-boosted or 2° gp100-boosted C57BL/6 mice. At day 8 after B16 injection, when tumors were palpable in all of the mice, 2° mice received the third immunization with either adenovirus (Ad)-gp100 or Ad-Ova. Naive mice remained unimmunized. Gp100 therapeutically vaccinated animals better controlled tumor growth (Figure 6E). At 18 days after vaccination, tumor size was reduced by ~61% compared to controls (Figure S5C). The effect was CD8 T cell mediated, as tumor growth was not controlled when CD8 T cells were depleted during vaccination (Figure S5D). Thus, therapeutic vaccination targeting self-specific CD8 T cells can delay malignant cell growth for established tumors.

Previous studies stressed the importance of neo-antigen-specific T cell responses in tumor control (Schumacher and Schreiber, 2015). To determine whether combination

immunotherapy generating both self- and neo-antigen-specific CD8 T cell responses could increase anti-tumor efficacy, we compared the anti-tumor potential of single- and dual-boosted mice. gp100 (self-Ag)- and Ova (neo-Ag)-specific T cell populations in C57BL/6 mice were generated by 3° immunizations. At day 2 after the final infection, single- and dual-antigen-boosted mice were challenged with B16-Ova melanoma tumors, which produce both gp100 (self) and Ova (neo) antigens. While single-boosted (Ova or gp100) T cell populations were able to delay tumor onset and protect 25%–30% of mice, the anti-tumor benefit was greatest for dual-boosted mice (Figure 6F). All (100%) of the dual-boosted mice remained tumor free for the duration of the study.

We predicted that synergism between self- and neo-antigen-specific T cell responses was responsible for increased tumor control in dual-boosted mice. This prediction was based on the paucity of total antigen-specific CD8 T cells in dual-boosted mice compared to single-boosted mice (Figure S5E). In the skin and SLOs, dual-boosted mice have fewer D^b-gp100- and K^b-SIINFEKL-specific CD8 T cells compared to their single-boosted counterparts. This may be linked to the decreased antigen load of each type during the dual-boosting process.

We showed that dual-boosting generated self- and neo-antigen-specific CD8 T cells in NLTs and SLOs (Figures 5G and S5A). The activation of T_{RM} *in situ* has been shown to recruit circulating immune cells and enhance immune activation and function locally (Beura et al., 2018; Schenkel et al., 2013). As circulating D^b-gp100-specific T cells are more functional than skin residents (Figure S4E), we hypothesized that self- and neo-antigen-specific CD8 T cells synergized by T_{RM} reactivation in the skin and inducing recruitment of circulating T cells. We tested the recruitment potential of skin T_{RM} in dual-boosted mice by tattooing the skin with cognate peptide—either gp100 or SIINFEKL. After *in situ* reactivation, K^b-SIINFEKL-specific CD8 T cells efficiently recruited circulating memory CD8 T cells (Figures 6G and S5F). Reactivated K^b-SIINFEKL-specific T_{RM} recruited CD4 T and natural killer (NK) cells, increased granzyme B, and recruited circulating D^b-gp100-specific cells (Figures 6G and S5G). This is similar to the observation that the reactivation of virus-specific CD8 T cells within tumors can enhance tumor elimination (Rosato et al., 2019). Therefore, both circulating and resident populations likely contribute to tumor control (Enamorado et al., 2017).

DISCUSSION

Our data show that established CD8 T cell tolerance is not absolute. Despite central and/or peripheral tolerance, responses to self- and shared tumor antigens can be elicited with sequential immunization targeting self-antigens *in vivo*. This method can generate functional self-specific CD8 T cells to different tissue-specific antigens. We show that even with AIRE-mediated negative selection, endogenous low-affinity self-specific CD8 T cells exist in the CD8 T cell repertoire. Multiple antigenic exposures drive antigen sensitization of self-specific CD8 T cells through avidity maturation, leading to MHC I tetramer binding, increased sensitivity to Ag, and expansion in peripheral blood, SLO, and NLT.

These data are supported by previous studies that demonstrated that transgenic, low-affinity self-specific CD8 T cells can escape negative selection in mice (Bouneaud et al., 2000; Zehn

and Bevan, 2006). We show that this is also true for endogenous self-specific CD8 T cells. We speculate that this would occur for many self-antigens. In humans, the negative selection of sex-specific CD8 T cells has been shown to be incomplete (Yu et al., 2015). Furthermore, rare CD8 T cells specific for shared self- and tumor-antigens can also be found within human colorectal tumors (Gee et al., 2018). Humans may harbor quiescent self-antigen-specific CD8 T cells, which could be exploited for immunotherapy.

Comparing tolerance to Ova in iFABP-Ova mice with gp100 in C57BL/6 mice, it is apparent that not all self-specific CD8 T cell responses are equal. While immunization enhanced both populations, the minimum number of boosting events differed. iFABP-Ova mice required three vaccinations and gp100 only two to observe self-specific T cell responses (Figures 2 and 5). We hypothesize that the difference observed in the two model systems might be due to variable T cell precursor frequency and TCR affinity (Rizzuto et al., 2009). The amount of antigen expressed in the thymus is important in determining precursor numbers (Sebzda et al., 1994). The density of MHC I-Ova complexes in iFABP-Ova mice and MHC I-gp100 in C57BL/6 mice may differ, and the amount of self-antigen expressed may vary between individuals. This could explain the variability in T cell burst size after 3° vaccination in iFABP-Ova mice (Figure 2D). Differences in PD-1 expression in each system may also be linked to TCR affinity (Jiang et al., 2016). We suspect that CD8 T cell tolerance to self-antigens and dysfunction in many contexts could be readily reversed, but the number of robust boosting events required to do this would vary because of precursor number and TCR affinity differences, which are influenced by the location and density of self-antigens.

Our data show that cumulative antigenic experience is key for the expansion of self-specific CD8 T cell populations and reversal of tolerance. Cell-intrinsic changes occur that allow self-specific T cells to bind MHC I tetramers, produce cytokines, and participate in antigen-specific killing. This type of population-level avidity maturation is key for the development of autoimmune diabetes and anti-tumor immunity (Amrani et al., 2000; Busch and Pamer, 1999; Slifka and Whitton, 2001; Xiang et al., 2017). These data suggest that increased antigen sensitivity is characteristic of T cells overcoming tolerance.

We have shown that with sequential immunization, self-antigens can be very immunogenic, and this method can generate large numbers of self-specific CD8 T cells. After 3° in iFABP-Ova mice, ~6×10^5 tetramer-binding self-specific CD8 T cells can be isolated from the spleen alone. This is an underestimate of the total self-specific CD8 T cell response, as antigen-specific T cells are found in other locations, and additional K^b-SIINFEKL-specific CD8 T cells are detectable with cytokine assays (Figure 3E). In naive C57BL/6 mice, the K^b-SIINFEKL precursor pool consists of ~125 cells (Obar et al., 2008). The starting frequency of K^b-SIINFEKL precursors in unmanipulated iFABP-Ova mice is unknown: it will likely be less than in C57BL/6 mice because of negative selection. Assuming no decrease in the precursor frequency in iFABP-Ova mice, the population of self-specific CD8 T cells expanded ~5,000 times based on MHC I tetramer counts and ~28,000 times based on cytokine counts (Figure 3E). gp100-specific CD8 T cell responses can also be as robust as foreign antigen-specific CD8 T cells, as demonstrated by the similar number of T cells in dually immunized mice (Figure S5A). This demonstrates that self-antigens are not

necessarily poorly immunogenic, but that immunization methods need to be robust and iterative to generate T cell responses to self.

We found that repeated immunizations with acute vectors are critical for tolerance reversal and cannot be replaced by a chronic infection, such as MCMV (Figure 4D). The rest period between immunizations may be crucial for the optimal expansion of self-specific CD8 T cells, as it is for foreign antigen-specific CD8 T cells (Thompson et al., 2016). This is likely important for the establishment of classical memory T cell characteristics, such as antigen-independent survival (Figure 4B) (Murali-Krishna et al., 1999; Swain et al., 1999).

This immunization regimen resulted in the widespread dissemination of self-specific CD8 T cells. Promiscuous seeding of numerous host organs is well established for foreign antigen-specific CD8 T cells (Masopust et al., 2001, 2004). Here, we show that OTI and melanocyte-specific T cells accumulated in all of the NLTs and SLOs that were analyzed (Figures S1 and S5A). In fact, the majority of boosted D^b-gp100-specific CD8 T cells were T_{RM} (Figure 5G). Proportionally, T_{RM} frequency is enhanced in the lung, liver, and small intestine after 3°. This is similar to what has been shown for sequential immunizations in the skin and may be particularly important for these organs, as they are highly vascularized and often sites of cancer metastases (Davies et al., 2017). Our immunization regimen also showed a trend toward increasing CD8 T_{RM} in SLOs (Schenkel et al., 2014; Tjin et al., 2011). This may be particularly important for cancer immunotherapy, as having cancer-specific T cells patrol LNs would be beneficial for metastasis control. The sufficiency of endogenously derived self-specific T_{RM} to control tumors bearing self-antigens warrants further investigation.

T_{RM} generated with multiple immunizations do not conform to the canonical $CD69^+CD103^+$ T_{RM} phenotype (Mackay et al., 2013; Steinert et al., 2015). Many self-specific T_{RM} express CD69, but expression varies across tissues. CD103 expression is lower in self-specific CD8 T cells compared to foreign antigen-specific CD8 T cells in the same tissues (Figure S6). CD103 downregulation may be linked to the frequency of antigen encounter and is not necessarily directly linked to tissue residency (Casey et al., 2012). This distinction is important, especially when examining human T_{RM}, which rely on phenotypic markers for classification. Our parabiosis data demonstrate that many self-specific CD8 T cells in intestinal and reproductive mucosal tissues are $CD103^-$ and some lack CD69. A re-examination of T_{RM} designation based on phenotypic markers is imminently needed.

These data also have important ramifications for cancer immunotherapy. Several groups have demonstrated that T_{RM} are crucial for effective tumor control and are correlated with increased survival (Enamorado et al., 2017; Malik et al., 2017; Nizard et al., 2017). Here, we show that melanocyte-specific CD8 T cells expanded through iterative immunization slow the growth of aggressive melanoma tumors in a therapeutic or prophylactic setting (Figure 6). The expansion of self-specific CD8 T cells did not result in pathology in healthy tissue. This is likely due to the difference in the amount of self-antigen produced in tumor tissue as compared to healthy tissue, yielding more MHC I-peptide complexes for CD8 T cells to engage when in tumors (Figures S5H and S5I). While D^b-gp100-specific CD8 T cells within tumors make IFN-γ and TNF-α, tumors are not always completely eliminated. However, additional rounds of immunization combined with concurrent boosting of neo-antigen-

specific CD8 T cells resulted in 100% tumor clearance (Figure 6F). The synergism observed between self- and neo-antigen-specific populations is not due to increased total tumor-specific cell numbers, as dual-boosted mice have fewer antigen-specific T cells compared to single-boosted mice. Upon *in situ* reactivation, K^b-SIINFEKL-specific CD8 T cells in the skin recruit and activate circulating immune cells (Figures 6G. S5F, and S5G). We hypothesize that neo-antigen-specific CD8 T cells synergize with self-specific populations by recruiting circulating tumor-reactive immune populations and generating a tumoricidal microenvironment (Schenkel et al., 2013). It is possible that targeting two tumor antigens prevents immune escape; however, the mutational landscape of B16-Ova tumors has not been explored in this context. These data show that self-specific CD8 T cells are an unrealized target for cancer immunotherapy and that these T cells can maximize anti-tumor responsiveness if complimenting neo-antigen-specific T cell responses (Lu and Robbins, 2016; Schumacher and Schreiber, 2015).

Heterologous prime-boost-boost could be used to reinvigorate dysfunctional tumor neo-antigen-specific CD8 T cells as well. Tolerant OTI in iFABP-Ova mice are very similar to dysfunctional tumor antigen-specific CD8 T cells (Figure 1) (Nelson et al., 2019; Pauken et al., 2015; Vezys and Lefrançois, 2002; Vezys et al., 2000). We have shown that tolerized OTI cells are resistant to single or combination checkpoint therapy, yet the immunization regimen presented here can induce expansion and functionality in these OTI (Figure 1) (Nelson et al., 2019; Pauken et al., 2015). Our data demonstrate that tolerant CD8 T cells resistant to checkpoint blockade can be rendered functional with robust, iterative antigenic stimulation and imply that this could activate T cells in cancer patients who do not respond to current immunotherapies.

Ultimately, tolerance to self-antigens can be overcome with repeated and robust antigen stimulation *in vivo*. Even dysfunctional high-affinity self-specific CD8 T cells resistant to checkpoint blockade can be rendered functional. Immunization targeting self-antigen induces T cell-intrinsic changes that confer improved antigen sensitivity and function with the deposition of large numbers of T_{RM} throughout the body. The robust expansion of host-specific CD8 T cells that recognize both self- and tumor antigens has therapeutic implications. We demonstrate that self-antigens are not necessarily poorly immunogenic, and their use as a cancer immunotherapy does not necessarily mean that autoimmune disease will be established. Ultimately, self-specific CD8 T cell populations are more dynamic and propitious than has been previously appreciated.

STAR★METHODS

LEAD CONTACT AND MATERIALS AVAILIBILITY

Information and requests for resources and reagents should be directed to and will be fulfilled by the Lead Contact, Vaiva Vezys (vvezys@umn.edu). This study did not generate any unique reagents.

EXPERIMENTAL MODEL AND SUBJECT DETAILS

Mice—C57BL/6J/CD45.2 (B6), B6.SJL-*Pfprc*^{a} *Pepc*^{b}/BoyJ (45.1), and B6.PL-*Thy1*^{a}/CyJ (B6 Thy1.1) mice were purchased from the Jackson Laboratory. OTI 45.1, OTI Thy1.1, P14, iFABP-Ova 45.2, and iFABP-Ova 45.1/45.2 mice were bred in our facility. Male and female mice were 6-12 weeks at the time of infection. Parabiosis studies only used female mice to prevent fighting. Littermates were randomly assigned into groups. All mice were used in accordance with University of Minnesota IACUC guidelines.

Cell Lines—Mycoplasma-free B16-F10 cells obtained from ATCC were expanded in RPMI 1640 with 10% FBS; 1% of the following: L-glutamine, penicillin/streptomycin, non-essential amino acids, and sodium pyruvate; and 1000× 2-mercaptoethanol. B16-Ova cells were obtained from B.J.B. and cultured similarly with the addition of G418 to maintain Ova expression. The sex of the B16-F10 or the B16-Ova cell lines is not known to us. Stocks were frozen and thawed at least 4 days prior to use. Cells were switched to DMEM containing media to induce melanin production at least 2 days prior to use.

METHOD DETAILS

Study Design—The research objectives of this study were to: (a) determine the steps necessary to stimulate a CD8 T cell response to self-antigen and (b) evaluate whether self-specific CD8 T cells are found within non-lymphoid tissues and can participate in tumor control. We hypothesized that repeated infections with heterologous replicating vectors expressing self-antigen would stimulate tolerant self-specific CD8 T cells to expand and participate in tumor control. This controlled laboratory study used three established mouse models to monitor tolerance in a population of CD8 T cells specific for self-antigen expressed in the small intestine (Vezys et al., 2000) and the skin (Enamorado et al., 2017; Malik et al., 2017; Nizard et al., 2017). Mice were randomly assigned to treatment groups where necessary. Sample size and endpoints were determined based on previous studies showing biological effects (Jiang et al., 2016; Malik et al., 2017). Data collection was terminated at pre-determined time points or when animal health or well-being was comprised, as determined by the University of Minnesota Institute for Animal Care and Use Committee (IACUC). All samples, including outliers, were included in the results.

Infections—Adult iFABP-Ova and B6 were immunized with 1×10^{6} PFU VSV-Ova i.v. (1°), 1×10^{4} CFU LM-Ova i.v. (2°), and/or 2×10^{6} PFU vaccinia virus (VV)-Ova i.v. (3°), with at least 30d between infections. The number of infections and infection type are indicated where necessary. Mice were immunized with MCMV-Ova i.p., as previously described (Snyder et al., 2008). For gp100 2° immunizations, adult C57BL/6 mice were immunized with 1×10^{6} PFU VSV-gp100 i.v. (1°) (Hailemichael et al., 2013) and 2×10^{8} PFU Ad2-gp100 (Sukumar et al., 2013) or Ad5-gp100 i.v (2°), with at least 30d between infections. For gp100 3° immunization, mice were given 1×10^{6} PFU VSV-gp100 i.v. (1°), 2×10^{6} PFU VV-gp100 i.v. (2°) and 2×10^{8} PFU Ad2-gp100 or Ad5-gp100 i.v (3°), with at least 30d between infections. For therapeutic vaccination experiments with Ova immunization, mice were given 1×10^{6} PFU VSV-Ova i.v. (1°), 2×10^{6} PFU VV-Ova i.v. (2°), and 2×10^{8} PFU Ad5-Ova i.v (3°). For dual infections with gp100 and OVA vectors, VSV was 1°, VV was used as 2° and Ad was used as a 3°, all i.v. Half the dose of the above stated

amounts was used for all dual infections, except Ad, which was given at the full amount. For 1 ° OTI memory experiments, OTI were transferred to congenically disparate C57BL/6 mice and infected with 1×10^6 PFU VSV-Ova i.v. the next day. For 1° P14 memory experiments, P14 were transferred to congenically disparate C57BL/6 mice and infected with 2×10^5 PFU LCMV-Armstrong i.p. the next day

Adoptive Transfers—Figure 4A: spleen and LN were harvested before 3° from iFABP-Ova/CD45.1/CD45.2 or B6/CD45.2 mice and incubated on plates coated with donkey-anti-mouse IgG F(ab')2 (H+L) and anti-CD4 (GK1.5) purified antibodies. Non-adherent cells were removed, washed, and transferred to naive iFABP-Ova/CD45.2 or B6/CD45.1 mice i.v. Mice were infected with VV-Ova 1d later.

Figure 4B: 5×10^5 K^b-SIINFEKL-specific CD8 T splenocytes from 3° boosted iFABP-Ova/CD45.2 mice were transferred i.v. to naive iFABP-Ova/CD45.1/CD45.2 or B6/CD45.1 mice.

Figures 1,5, S1, and S2: B6 memory OTI - 5×10^5 naive OTI/CD45.1 or OTI/CD90.1+ splenocytes were transferred i.v. to C57BL/6/CD45.2 mice and infected the next day. OTI tolerance experiments: 5×10^5 naive OTI/CD45.1 splenocytes were transferred i.v. to iFABP-Ova/CD45.2 mice or B6/CD45.2 mice and maintained for at least 30 days before sacrifice or infection for iFABP-Ova. B6 were infected within 2 days of OTI transfer because of naive T cell lifespan (Nelson et al., 2019; Pauken et al., 2015).

Isolation of Lymphocytes, ELISA, and Flow Cytometry—Lymphocytes from the spleen, LN, PBL, female reproductive tract (FRT), liver, lung, salivary gland (SG) and small intestinal intraepithelial layer were isolated as previously described (Steinert et al., 2015). Brains were chopped and stirred 1h at 37°C with 100 U/mL type I collagenase (Worthington, Lakewood, NJ). All single cell suspensions were separated using 44/67% Percoll density gradients. Hair was removed from a $4cm^2$ abdominal skin section, chopped, and stirred in 2U/mL DNase, and 3mg/mL type III collagenase for 1h at 37°C (Mackay et al., 2013). Tumors were chopped and stirred in 2U/mL DNase and 100U/mL type I collagenase for 15 m at 37°C. Tetramer pulldown was not performed on CD8 T cells, except for some data in Figures 5B and 6A. Surface stains and intracellular stains were performed as previously described (Masopust et al., 2006). Samples were acquired on an LSRII. Tissue and blood compartments were distinguished by i.v. injection of anti-CD8α antibody (Anderson et al., 2012). Serum iFABP was measured by a Mouse iFABP ELISA Kit.

Cytotoxicity and Cytokine Assays—*In vivo* cytotoxicity assay: Naive splenocytes were labeled with 1 μM (Hi) or 100nM (Lo) CFSE (Barber et al., 2003). CFSE-Lo cells were pulsed with 1 μM SIINFEKL. Equal numbers of peptide-pulsed and non-pulsed cells were transferred i.v. to naive, 1° or 3° mice. 4h later, spleens were harvested. Percent killing calculation: 100-([(% peptide pulsed in boosted/% non-pulsed in boosted)/(% peptide pulsed in naive/% non-pulsed in naive)]×100). For cytokine production, lymphocytes were incubated with 1 μg/mL GolgiPlug with or without 1 μg/mL peptide for OTI and gp100 experiments, 10-100 μg/mL peptide for endogenous Ova for 4h at 37°C.

Thymectomy—Adult mice were anesthetized and a lateral incision was made through skin and the top of the sternum to visualize the thymus. The thymus was extracted via vacuum and the wound was sutured. Animals recovered for 6 weeks before any other experimental procedures were performed.

Histology—Hematoxylin and eosin staining was performed on formalin fixed sections of small intestine. H&E staining was also performed on frozen skin sections. Sections were evaluated by a veterinary pathologist.

Parabiosis—Parabiosis surgery was done as described (Schenkel et al., 2013). Each mouse was shaved along the opposite lateral flank. Identical incisions were made on the lateral aspect of each mouse, and mice were conjoined via skin staples. Parabiosed mice were then allowed to rest for 14–30 days before sacrifice. Equilibration was confirmed in the peripheral blood prior to sacrifice. Percent residence formula: 100 × (1-((# donor Ag-specific × 2)/(donor Ag-specific + host Ag-specific))).

Tumor Challenges—B6 mice were immunized and at day 2 after 2°, mice were challenged with 1×10^5 B16/F10 or B16-Ova cells s.c. In prophylactic experiments, B16-Ova was given at day 2 after 2° or 3°. For therapeutic experiments, B16 cells were injected s.c. and at day 8 of B16 growth, when tumors were palpable, mice were (or were not) injected with Ad-Ova or Ad-gp100. For checkpoint blockade, anti-PD-L1 antibody was given at the time of the prophylactic vaccination, and then every 3 days at 200 μg i.p. for the duration of the tumor experiment. For CD8 depletion, anti-CD8 antibody was given after tumor challenge at 200 μg i.p. the day before therapeutic vaccination and at days 2 and 4.

Skin Recruitment—Skin recruitment was analyzed by tattooing 4 μg of indicated peptide in 50 μL volume at 20mm depth on shaved and depilated skin, and recruitment was assessed 48h later with the skin isolation protocol above. For recruitment of circulating memory cells, CD45.1 + memory P14 were enriched from the spleen 30 days after LCMV infection using CD8 negative selection and lymphocytes were transferred i.v. to dual-boosted hosts. The next day, hosts were tattooed with SIINFEKL orgp100 peptide. For recruitment of endogenous cell populations, dual-boosted mice were tattooed with SIINFEKL and gp100 on opposite flanks. For recruitment of D^b-gp100-specific CD8 T cells, 3° gp100-boosted splenocytes were enriched for CD8 T cells and transferred to 3° dual-boosted mice, and the next day mice were tattooed with SIINFEKL peptide. Control depilation was done on contralateral side where indicated.

Immunohistochemistry—Frozen tumors with adjacent healthy skin were cut into 7 μm sections, mounted on glass slides, air-dried and fixed in acetone. Rabbit anti-mouse gp100 antibody was added after a blocking step, goat-α-rabbit Ig was used as the secondary antibody with a DAPI counterstain. Fluorescence was acquired on a Leica DM5500B 4 color fluorescent system with motorized z-focus stage for fully automated image stitching. Enumeration of gp100+ cells was done manually in ImageJ64. Representative areas in tumor and skin were selected and ImageJ64 software was used to enumerate DAPI+ nuclei (Steinert et al., 2015). In the same image, gp100+ cells were determined by manual counting. To determine gp100 fluorescence per cell, a representative area on the tumor was

selected and ImageJ64 software was used to calculate the integrated density and area of individual gp-100+ tumor cells. Similar gp-100 enumeration was done after selecting a representative area on the skin. Background readings of mean fluorescence were collected by selecting an area of the image where no cells were present. Corrected total cell fluorescence (CTCF) was calculated using this formula: CTCF = Integrated Density – (Area of selected cell X Mean fluorescence of background reading).

QUANTIFICATION AND STATISTICAL ANALYSIS

For bar graphs, error bars indicated ± SEM, except in Figure 3 where ± SD was used, as indicated. All samples were included, including outliers. For all figures, n refers to animal subjects, except Figure S5I top panel, where n refers to individual cells. Number of animals for each figure is indicated in the figure legend. Two-tailed t tests, Mann-Whitney U tests or Kruskal-Wallis H tests were performed where appropriate. Kaplan-Meier curves used Mantel-Cox test for significance. For all analyses, p values of less than 0.05 were considered significant. Star representation is indicated in figure legends.

DATA AND CODE AVAILIBILITY

This study did not generate datasets/code.

Supplementary Material

Refer to Web version on PubMed Central for supplementary material.

ACKNOWLEDGMENTS

We would like to thank Drs. Victor Engelhard, Thomas Griffith, Zong Sheng Guo, Ann Hill, Marc Jenkins, Nicholas Restifo, and Kimberly Schluns for reagents. This work was supported by NIH grant DP2OD006472 (to V.V.), agrant from the Randy Shaver Cancer Research and Community Fund (to V.V.), and NIH grant T32AI007313 (to C.E.N. and E.A.T.).

REFERENCES

Amrani A, Verdaguer J, Serra P, Tafuro S, Tan R, and Santamaria P (2000). Progression of autoimmune diabetes driven by avidity maturation of a T-cell population. Nature 406, 739–742. [PubMed: 10963600]

Anderson KG, Sung H, Skon CN, Lefrancois L, Deisinger A, Vezys V, and Masopust D (2012). Cutting edge: intravascular staining redefines lung CD8 T cell responses. J. Immunol 189, 2702–2706. [PubMed: 22896631]

Barber DL, Wherry EJ, and Ahmed R (2003). Cutting edge: rapid in vivo killing by memory CD8 T cells. J. Immunol 171, 27–31. [PubMed: 12816979]

Beura LK, Mitchell JS, Thompson EA, Schenkel JM, Mohammed J, Wijeyesinghe S, Fonseca R, Burbach BJ, Hickman HD, Vezys V, et al. (2018). Intravital mucosal imaging of $CD8^+$ resident memory T cells shows tissue-autonomous recall responses that amplify secondary memory. Nat. Immunol 19, 173–182. [PubMed: 29311694]

Boddupalli CS, Bar N, Kadaveru K, Krauthammer M, Pornputtapong N, Mai Z, Ariyan S, Narayan D, Kluger H, Deng Y, et al. (2016). Interlesional diversity of T cell receptors in melanoma with immune checkpoints enriched in tissue-resident memory T cells. JCI Insight 1, e88955. [PubMed: 28018970]

Bouneaud C, Kourilsky P, and Bousso P (2000). Impact of negative selection on the T cell repertoire reactive to a self-peptide: a large fraction of T cell clones escapes clonal deletion. Immunity 13, 829–840. [PubMed: 11163198]

Busch DH, and Pamer EG (1999). T cell affinity maturation by selective expansion during infection. J. Exp. Med 189, 701–710. [PubMed: 9989985]

Casey KA, Fraser KA, Schenkel JM, Moran A, Abt MC, Beura LK, Lucas PJ, Artis D, Wherry EJ, Hogquist K, et al. (2012). Antigen-independent differentiation and maintenance of effector-like resident memory T cells in tissues. J. Immunol 188, 4866–4875. [PubMed: 22504644]

Cho HI, Jung SH, Sohn HJ, Celis E, and Kim TG (2015). An optimized peptide vaccine strategy capable of inducing multivalent $CD8^+$ T cell responses with potent antitumor effects. OncoImmunology 4, e1043504. [PubMed: 26451316]

Davies B, Prier JE, Jones CM, Gebhardt T, Carbone FR, and Mackay LK (2017). Cutting Edge: Tissue-Resident Memory T Cells Generated by Multiple Immunizations or Localized Deposition Provide Enhanced Immunity. J. Immunol 198, 2233–2237. [PubMed: 28159905]

Derikx JP, Vreugdenhil AC, Van den Neucker AM, Grootjans J, van Bijnen AA, Damoiseaux JG, van Heurn LW, Heineman E, and Buurman WA (2009). A pilot study on the noninvasive evaluation of intestinal damage in celiac disease using I-FABP and L-FABP. J. Clin. Gastroenterol 43, 727–733. [PubMed: 19359998]

Enamorado M, Iborra S, Priego E, Cueto FJ, Quintana JA, Martinez-Cano S, Mejías-Pérez E, Esteban M, Melero I, Hidalgo A, and Sancho D (2017). Enhanced anti-tumour immunity requires the interplay between resident and circulating memory $CD8^+$ T cells. Nat. Commun 8, 16073. [PubMed: 28714465]

Enouz S, Carrié L, Merkler D, Bevan MJ, and Zehn D (2012). Autoreactive T cells bypass negative selection and respond to self-antigen stimulation during infection. J. Exp. Med 209, 1769–1779. [PubMed: 22987800]

Gee MH, Han A, Lofgren SM, Beausang JF, Mendoza JL, Birnbaum ME, Bethune MT, Fischer S, Yang X, Gomez-Eerland R, et al. (2018). Antigen Identification for Orphan T Cell Receptors Expressed on Tumor-Infiltrating Lymphocytes. Cell 172, 549–563.e16. [PubMed: 29275860]

Hailemichael Y, Dai Z, Jaffarzad N, Ye Y, Medina MA, Huang XF, Dorta-Estremera SM, Greeley NR, Nitti G, Peng W, et al. (2013). Persistent antigen at vaccination sites induces tumor-specific $CD8^+$ T cell sequestration, dysfunction and deletion. Nat. Med 19, 465–472. [PubMed: 23455713]

Hernández J, Lee PP, Davis MM, and Sherman LA (2000). The use of HLA A2.1/p53 peptide tetramers to visualize the impact of self tolerance on the TCR repertoire. J. Immunol 164, 596–602. [PubMed: 10623800]

Irvine KR, Chamberlain RS, Shulman EP, Surman DR, Rosenberg SA, and Restifo NP (1997). Enhancing efficacy of recombinant anticancer vaccines with prime/boost regimens that use two different vectors. J. Natl. Cancer Inst 89, 1595–1601. [PubMed: 9362157]

Ji Q, Perchellet A, and Goverman JM (2010). Viral infection triggers central nervous system autoimmunity via activation of CD8+ T cells expressing dual TCRs. Nat. Immunol 11, 628–634. [PubMed: 20526343]

Jiang TT, Martinov T, Xin L, Kinder JM, Spanier JA, Fife BT, and Way SS (2016). Programmed Death-1 Culls Peripheral Accumulation of High-Affinity Autoreactive CD4 T Cells to Protect against Autoimmunity. Cell Rep. 17, 1783–1794. [PubMed: 27829150]

Kawakami Y, Eliyahu S, Jennings C, Sakaguchi K, Kang X, Southwood S, Robbins PF, Sette A, Appella E, and Rosenberg SA (1995). Recognition of multiple epitopes in the human melanoma antigen gp100 by tumor-infiltrating T lymphocytes associated with in vivo tumor regression. J. Immunol 154, 3961–3968. [PubMed: 7706734]

Larkin J, Chiarion-Sileni V, Gonzalez R, Grob JJ, Cowey CL, Lao CD, Schadendorf D, Dummer R, Smylie M, Rutkowski P, et al. (2015). Combined Nivolumab and Ipilimumab or Monotherapy in Untreated Melanoma. N. Engl. J. Med 373, 23–34. [PubMed: 26027431]

Lee JW, Epardaud M, Sun J, Becker JE, Cheng AC, Yonekura AR, Heath JK, and Turley SJ (2007). Peripheral antigen display by lymph node stroma promotes T cell tolerance to intestinal self. Nat. Immunol 8, 181–190. [PubMed: 17195844]

Lu YC, and Robbins PF (2016). Cancer immunotherapy targeting neoantigens. Semin. Immunol 28, 22–27. [PubMed: 26653770]

Mackay LK, Rahimpour A, Ma JZ, Collins N, Stock AT, Hafon ML, Vega-Ramos J, Lauzurica P, Mueller SN, Stefanovic T, et al. (2013). The developmental pathway for CD103(+)CD8+ tissue-resident memory T cells of skin. Nat. Immunol 14, 1294–1301. [PubMed: 24162776]

Malik BT, Byrne KT, Vella JL, Zhang P, Shabaneh TB, Steinberg SM, Molodtsov AK, Bowers JS, Angeles CV, Paulos CM, et al. (2017). Resident memory T cells in the skin mediate durable immunity to melanoma. Sci. Immunol 2, eaam6346.

Masopust D, Vezys V, Marzo AL, and Lefrançois L (2001). Preferential localization of effector memory cells in nonlymphoid tissue. Science 291, 2413–2417. [PubMed: 11264538]

Masopust D, Vezys V, Usherwood EJ, Cauley LS, Olson S, Marzo AL, Ward RL, Woodland DL, and Lefrançois L (2004). Activated primary and memory CD8 T cells migrate to nonlymphoid tissues regardless of site of activation or tissue of origin. J. Immunol 172, 4875–4882. [PubMed: 15067066]

Masopust D, Ha SJ, Vezys V, and Ahmed R (2006). Stimulation history dictates memory CD8 T cell phenotype: implicationsfor prime-boost vaccination. J. Immunol 177, 831–839. [PubMed: 16818737]

McGranahan N, and Swanton C (2017). Clonal Heterogeneity and Tumor Evolution: Past, Present, and the Future. Cell 168, 613–628. [PubMed: 28187284]

Mueller DL (2010). Mechanisms maintaining peripheral tolerance. Nat. Immunol 11, 21–27. [PubMed: 20016506]

Murali-Krishna K, Lau LL, Sambhara S, Lemonnier F, Altman J, and Ahmed R (1999). Persistence of memory CD8 T cells in MHC class I-deficient mice. Science 286, 1377–1381. [PubMed: 10558996]

Nelson CE, Mills LJ, McCurtain JL, Thompson EA, Seelig DM, Bhela S, Quarnstrom CF, Fife BT, and Vezys V (2019). Reprogramming responsiveness to checkpoint blockade in dysfunctional CD8 T cells. Proc. Natl. Acad. Sci. USA 116, 2640–2645. [PubMed: 30679280]

Nizard M, Roussel H, Diniz MO, Karaki S, Tran T, Voron T, Dransart E, Sandoval F, Riquet M, Rance B, et al. (2017). Induction of resident memory T cells enhances the efficacy of cancer vaccine. Nat. Commun 8, 15221. [PubMed: 28537262]

Obar JJ, Khanna KM, and Lefrançois L (2008). Endogenous naive CD8+ T cell precursor frequency regulates primary and memory responses to infection. Immunity 28, 859–869. [PubMed: 18499487]

Overwijk WW, Tsung A, Irvine KR, Parkhurst MR, Goletz TJ, Tsung K, Carroll MW, Liu C, Moss B, Rosenberg SA, and Restifo NP (1998). gp100/pmel 17 is a murine tumor rejection antigen: induction of “self”-reactive, tumoricidal T cells using high-affinity, altered peptide ligand. J. Exp. Med 188, 277–286. [PubMed: 9670040]

Overwijk WW, Lee DS, Surman DR, Irvine KR, Touloukian CE, Chan CC, Carroll MW, Moss B, Rosenberg SA, and Restifo NP (1999). Vaccination with a recombinant vaccinia virus encoding a “self” antigen induces autoimmune vitiligo and tumor cell destruction in mice: requirement for CD4(+) T lymphocytes. Proc. Natl. Acad. Sci. USA 96, 2982–2987. [PubMed: 10077623]

Pauken KE, Nelson CE, Martinov T, Spanier JA, Heffernan JR, Sahli NL, Quarnstrom CF, Osum KC, Schenkel JM, Jenkins MK, et al. (2015). Cutting edge: identification of autoreactive CD4+ and CD8+ T cell subsets resistant to PD-1 pathway blockade. J. Immunol 194, 3551–3555. [PubMed: 25769925]

Philip M, Fairchild L, Sun L, Horste EL, Camara S, Shakiba M, Scott AC, Viale A, Lauer P, Merghoub T, et al. (2017). Chromatin states define tumour-specific T cell dysfunction and reprogramming. Nature 545, 452–456. [PubMed: 28514453]

Rizzuto GA, Merghoub T, Hirschhorn-Cymerman D, Liu C, Lesokhin AM, Sahawneh D, Zhong H, Panageas KS, Perales MA, Altan-Bonnet G, et al. (2009). Self-antigen-specific CD8+ T cell precursor frequency determines the quality of the antitumor immune response. J. Exp. Med 206, 849–866. [PubMed: 19332877]

Rosato PC, Wijeyesinghe S, Stolley JM, Nelson CE, Davis RL, Manlove LS, Pennell CA, Blazar BR, Chen CC, Geller MA, et al. (2019). Virus-specific memory T cells populate tumors and can be repurposed for tumor immunotherapy. Nat. Commun 10, 567. [PubMed: 30718505]

Sathaliyawala T, Kubota M, Yudanin N, Turner D, Camp P, Thome JJ, Bickham KL, Lerner H, Goldstein M, Sykes M, et al. (2013). Distribution and compartmentalization of human circulating and tissue-resident memory T cell subsets. Immunity 38, 187–197. [PubMed: 23260195]

Schenkel JM, Fraser KA, Vezys V, and Masopust D (2013). Sensing and alarm function of resident memory $CD8^+$ T cells. Nat. Immunol 14, 509–513. [PubMed: 23542740]

Schenkel JM, Fraser KA, and Masopust D (2014). Cutting edge: resident memory CD8 T cells occupy frontline niches in secondary lymphoid organs. J. Immunol 192, 2961–2964. [PubMed: 24600038]

Schietinger A, Delrow JJ, Basom RS, Blattman JN, and Greenberg PD (2012). Rescued tolerant CD8 T cells are preprogrammed to reestablish the tolerant state. Science 335, 723–727. [PubMed: 22267581]

Schietinger A, Philip M, Krisnawan VE, Chiu EY, Delrow JJ, Basom RS, Lauer P, Brockstedt DG, Knoblaugh SE, Hämmerling GJ, et al. (2016). Tumor-Specific T Cell Dysfunction Is a Dynamic Antigen-Driven Differentiation Program Initiated Early during Tumorigenesis. Immunity 45, 389–401. [PubMed: 27521269]

Schumacher TN, and Schreiber RD (2015). Neoantigens in cancer immunotherapy. Science 348, 69–74. [PubMed: 25838375]

Sebzda E, Wallace VA, Mayer J, Yeung RS, Mak TW, and Ohashi PS (1994). Positive and negative thymocyte selection induced by different concentrations of a single peptide. Science 263, 1615–1618. [PubMed: 8128249]

Slifka MK, and Whitton JL (2001). Functional avidity maturation of CD8(+) T cells without selection of higher affinity TCR. Nat. Immunol 2, 711–717. [PubMed: 11477407]

Snyder CM, Cho KS, Bonnett EL, van Dommelen S, Shellam GR, and Hill AB (2008). Memory inflation during chronic viral infection is maintained by continuous production of short-lived, functional T cells. Immunity 29, 650–659. [PubMed: 18957267]

Steinert EM, Schenkel JM, Fraser KA, Beura LK, Manlove LS, Igyártó BZ, Southern PJ, and Masopust D (2015). Quantifying Memory CD8 T Cells Reveals Regionalization of Immunosurveillance. Cell 161, 737–749. [PubMed: 25957682]

Sukumar M, Liu J, Ji Y, Subramanian M, Crompton JG, Yu Z, Roychoudhuri R, Palmer DC, Muranski P, Karoly ED, et al. (2013). Inhibiting glycolytic metabolism enhances CD8+ T cell memory and antitumor function. J. Clin. Invest 123, 4479–4488. [PubMed: 24091329]

Swain SL, Hu H, and Huston G (1999). Class II-independent generation of CD4 memory T cells from effectors. Science 286, 1381–1383. [PubMed: 10558997]

Thompson EA, Beura LK, Nelson CE, Anderson KG, and Vezys V (2016). Shortened Intervals during Heterologous Boosting Preserve Memory CD8 T Cell Function but Compromise Longevity. J. Immunol 196, 3054–3063. [PubMed: 26903479]

Tjin EP, Konijnenberg D, Krebbers G, Mallo H, Drijfhout JW, Franken KL, van der Horst CM, Bos JD, Nieweg OE, Kroon BB, et al. (2011). T-cell immune function in tumor, skin, and peripheral blood of advanced stage melanoma patients: implications for immunotherapy. Clin. Cancer Res 17, 5736–5747. [PubMed: 21750202]

Vezys V, and Lefrançois L (2002). Cutting edge: inflammatory signals drive organ-specific autoimmunity to normally cross-tolerizing endogenous antigen. J. Immunol 169, 6677–6680. [PubMed: 12471097]

Vezys V, Olson S, and Lefrançois L (2000). Expression of intestine-specific antigen reveals novel pathways of CD8 T cell tolerance induction. Immunity 12, 505–514. [PubMed: 10843383]

Wakim LM, Woodward-Davis A, and Bevan MJ (2010). Memory T cells persisting within the brain after local infection show functional adaptations to their tissue of residence. Proc. Natl. Acad. Sci. USA 107, 17872–17879. [PubMed: 20923878]

Wherry EJ, Barber DL, Kaech SM, Blattman JN, and Ahmed R (2004). Antigen-independent memory CD8 T cells do not develop during chronic viral infection. Proc. Natl. Acad. Sci. USA 101, 16004–16009. [PubMed: 15505208]

Xiang B, Baybutt TR, Berman-Booty L, Magee MS, Waldman SA, Alexeev VY, and Snook AE (2017). Prime-Boost Immunization Eliminates Metastatic Colorectal Cancer by Producing High-Avidity Effector $CD8^+$ T Cells. J. Immunol 198, 3507–3514. [PubMed: 28341670]

Yu W, Jiang N, Ebert PJ, Kidd BA, Müller S, Lund PJ, Juang J, Adachi K, Tse T, Birnbaum ME, et al. (2015). Clonal Deletion Prunes but Does Not Eliminate Self-Specific αβ CD8(+) T Lymphocytes. Immunity 42, 929–941. [PubMed: 25992863]

Zehn D, and Bevan MJ (2006). T cells with low avidity for a tissue-restricted antigen routinely evade central and peripheral tolerance and cause autoimmunity. Immunity 25, 261–270. [PubMed: 16879996]

Highlights

- Iterative stimulation with antigen and inflammation reverses $CD8^+$ T cell tolerance
- Tolerance reversal results in avidity maturation and enhanced antigen sensing
- Expanded self-specific $CD8^+$ T cells form T_{RM} in lymphoid and non-lymphoid tissues
- Self-specific $CD8^+$ T cells control tumor growth without concomitant autoimmunity

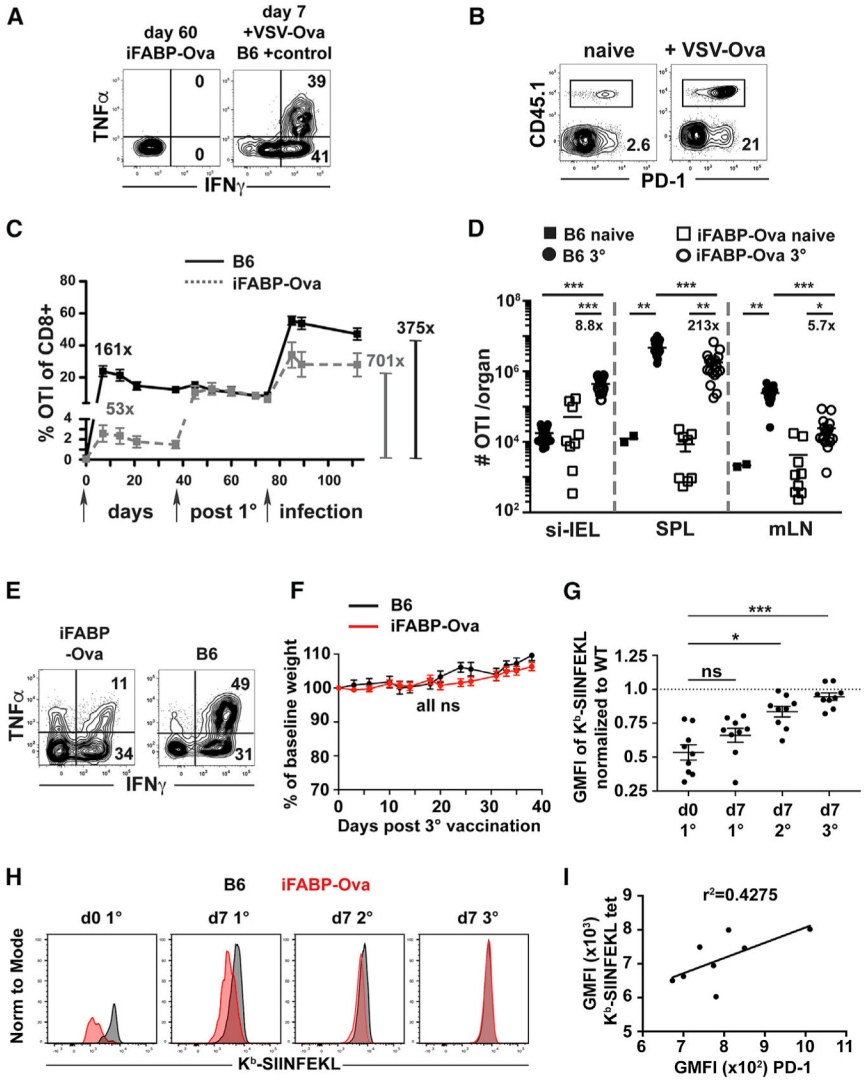

Figure 1. Robust Immunization Overcomes Peripheral Tolerance of Dysfunctional High-Affinity Self-Specific CD8 T Cells

(A) IFN-γ and TNF-α production by OTI from small intestine intraepithelial lymphocyte (IEL) compartment after *ex vivo* peptide stimulation. Left (tolerant): 60 days after adoptive transfer in iFABP-Ova hosts. Right (effector): day 7 after VSV-Ova in C57BL/6 hosts. Plots are gated on OTI.

(B) iFABP-Ova mice were (+VSV-Ova) or were not (naive) infected with VSV-Ova 72 days after transfer of OTI. IELs were analyzed 359 days after OTI transfer. Plots are gated on i.v. negative $CD8^+$ T cells. Numbers represent the frequency in gate.

(C) OTI in PBL after day 0 of 1° (VSV-Ova) infection in B6 and iFABP-Ova mice. IFABP-Ova mice were infected 60 days after OTI transfer. B6 mice were infected 2 days after OTI transfer. The arrows indicate immunization (1° VSV-Ova; 2° LM-Ova; 3° VV-Ova). Solid black, B6; dashed gray, iFABP-Ova. Numbers, fold expansion of OTI at day 7 after 1° and day 7 after 3°, relative to day 0.

(D) Number of OTI without infection (naive) and at days 30–40 post-3° in the IEL, spleen (SPL), and mLN. Filled, B6; open, iFABP-Ova; square, unimmunized; circle, after 3°.

Numbers on graph, fold expansion from naive to 3°. Naive B6 IELs not included, as naive T cells are not found in NLTs.

(E) IFN-γ and TNF-α production by splenic OTI 7 days after 3° in B6 and iFABP-Ova after *ex vivo* peptide stimulation. Plots are gated on OTI.

(F) Weight of B6 and iFABP-Ova mice after 3°. Black, B6; red, iFABP-Ova.

(G) Geometric mean fluorescence intensity (GMFI) of K^b-SIINFEKL tetramer staining of OTI in PBLs of iFABP-Ova mice at indicated time points, normalized to wild type.

(H) Histograms of K^b-SIINFEKL tetramer staining of the OTI enumerated in (G). Black, B6 OTI. Red, iFABP-Ova OTI.

(I) Correlation of GMFI of K^b-SIINFEKL tetramer staining and GMFI PD-1 on OTI from iFABP-Ova mice day 6 after 3° in PBL. R^2 value = 0.04275.

Representative of at least 2 experiments totaling 3–10 animals per group. *p ≤ 0.037, **p ≤ 0.007, ***p ≤ 0.0002. Error bars indicate means ± SEMs.

See also Figures S1 and S2.

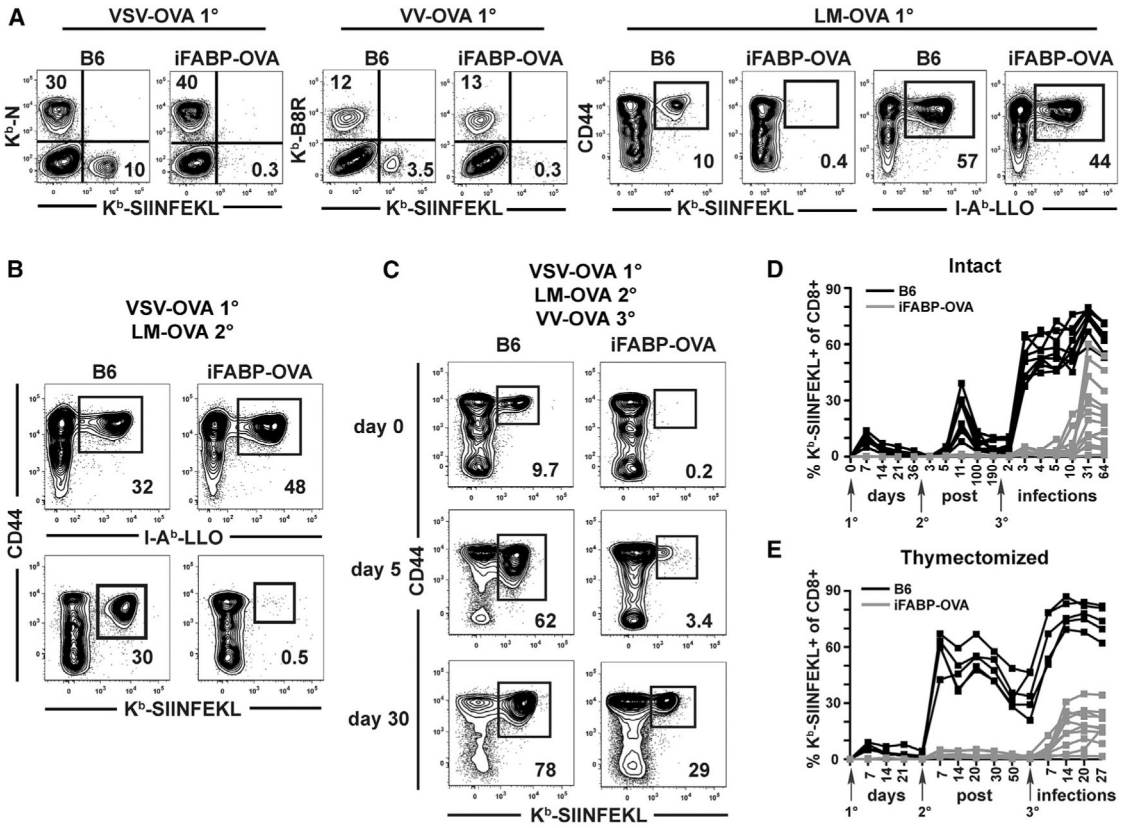

Figure 2. Sequential Immunization Induces Responsiveness in Endogenous Self-Specific CD8 T Cells

(A) IFABP-Ova and B6 mice were infected with VSV-Ova, VV-Ova, or LM-Ova only. PBLs were analyzed 7 days later for K^b-SIINFEKL-, K^b-N-, or K^b-B8R-specific CD8 T cells, or splenocytes were analyzed for I-A^b-listeriolysin O (LLO)-specific CD4 T cells. N, B8R, and LLO epitopes from VSV, VV, or LM vector proteins. Gated on CD8 or CD4 T cells, respectively.

(B) IFABP-Ova and B6 mice were infected with VSV-Ova and then LM-Ova 60 days later. I-A^b-LLO-specific CD4 or K^b-SIINFEKL-specific CD8 T cells were enumerated 7 days after LM-Ova. Top: splenocytes gated on CD4 T cells. Bottom: PBLs gated on CD8 T cells.

(C–E) IFABP-Ova and B6 mice were infected with VSV-Ova, LM-Ova, and VV-Ova at least 40 days apart.

(C) K^b-SIINFEKL-specific CD8 T cells in PBLs of the same animal at the indicated times after VV-Ova (3°). Gated on CD8 T cells.

(D) K^b-SIINFEKL-specific CD8 T cells in PBLs were enumerated over the immunization period. Gray, iFABP-Ova; black, B6. Each line represents an individual.

(E) K^b-SIINFEKL-specific CD8 T cells in PBLs were enumerated as in (D) in adult mice thymectomized before 1°.

Representative of at least 2 experiments totaling 5–12 animals per group.

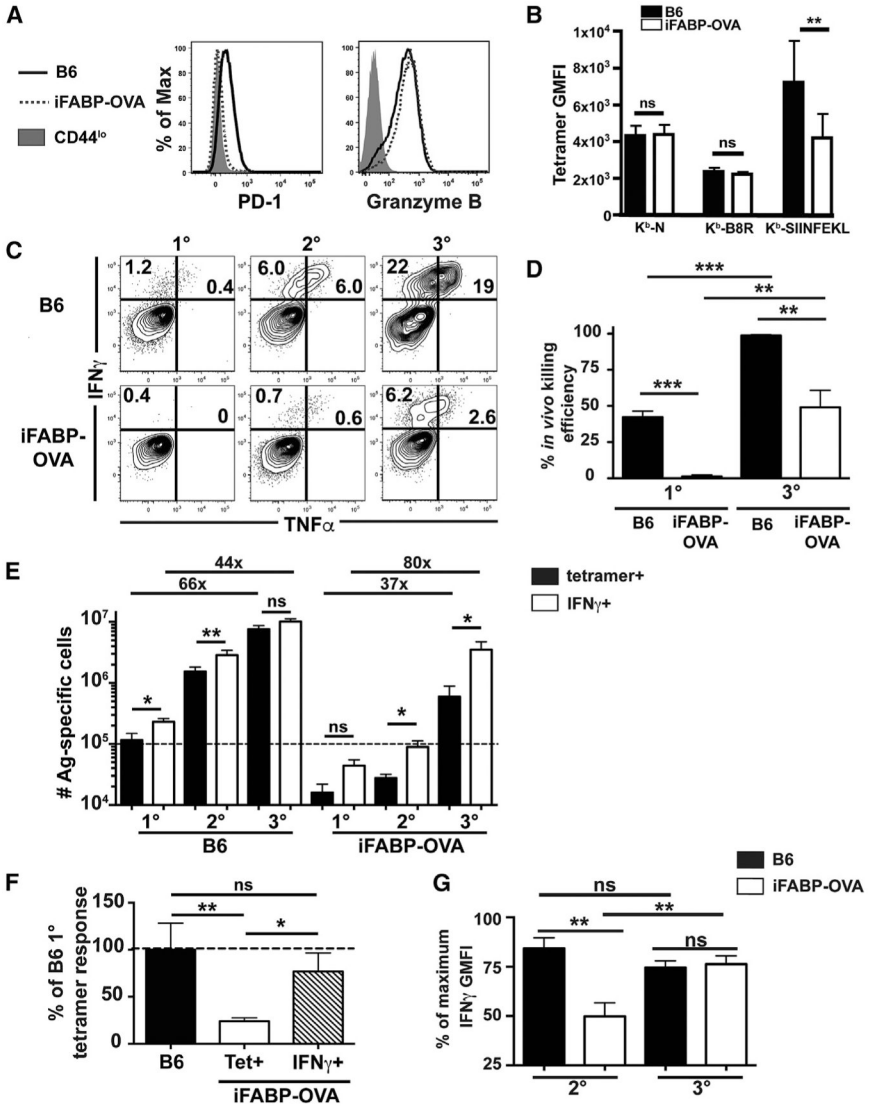

Figure 3. Sequential Immunization Drives Avidity Maturation of Functional, Endogenous Self-Specific CD8 T Cells

B6 or iFABP-Ova mice were subjected to Ova immunization.

(A) PD-1 and granzyme B expression by K^b-SIINFEKL-specific splenocytes 35 days post-3°. Histograms are gated on K^b-SIINFEKL-specific CD8 T cells from iFABP-Ova (dashed) and B6 (solid) or $CD44^{lo}$ CD8 T cells (gray filled).

(B) GMFIs of indicated MHC I tetramer staining in splenocytes of iFABP-Ova (white) or B6 (black) mice at least 30 days after 3° VV-Ova.

(C) Splenocyte IFN-γ and TNF-α production with *ex vivo* peptide stimulation ≥30 days after 1°, 2°, or 3°. Plots are gated on CD8 T cells.

(D) *In vivo* killing of SIINFEKL-pulsed target cells 30 days post-1° or 3°. Black, B6; white, iFABP-Ova.

(E) Enumeration of splenocytes binding K^b-SIINFEKL tetramer or producing IFN-γ ≥30 days after 1°, 2°, or 3°. Black, $tetramer^+$; white, IFN-γ. The dotted line represents CD8 T cells readily detectable in B6 at 1° with K^b-SIINFEKL tetramers.

(F) K^b-SIINFEKL-specific CD8 T cell responses detected either with MHC I tetramer staining (Tet^+) or cytokine assay (IFN-γ^+) in iFABP-Ova mice after 2° as a function of K^b-SIINFEKL tetramer-binding cells in B6 mice after 1°.

(G) Percentage of maximum IFN-γ produced by splenic CD8 T cells ≥ 30 days after 2° or 3°. GMFI of IFN-γ production at 2° or 3° normalized to maximum GMFI of IFN-γ at matching time point. Black, B6; white, iFABP-Ova.

Representative of at least 2 experiments totaling 4–12 animals per group. *$p < 0.037$, **$p \leq 0.009$, ***$p \leq 0.0006$. Error bars indicate means ± SEMs, except in (B) where it is SDs. See also Figure S3.

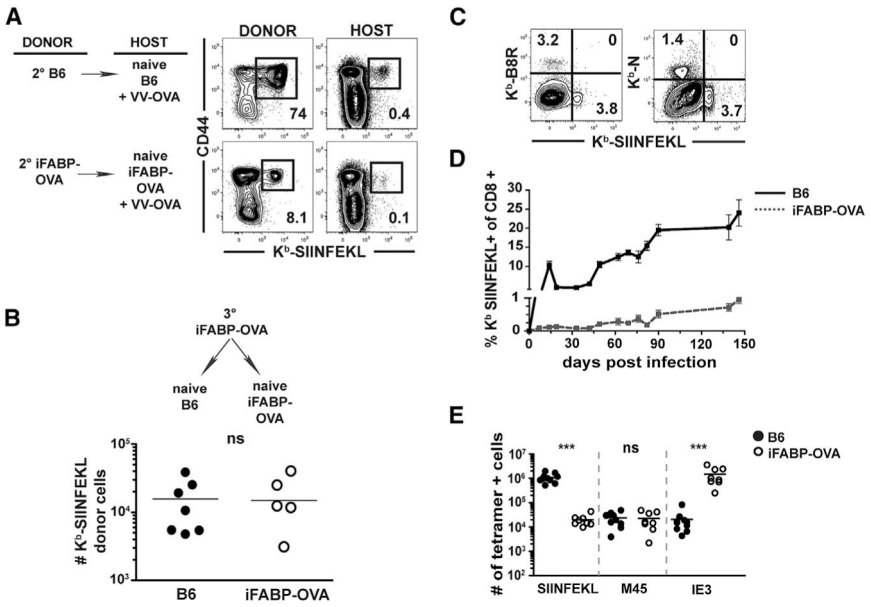

Figure 4. Sequential Immunization Induces Cell-Intrinsic Changes in Self-Specific CD8 T Cells with Memory T Cell Characteristics

(A) Splenocytes from iFABP-Ova or B6 mice before 3° were transferred into naive, congenically mismatched iFABP-Ova or B6, respectively. Host mice were infected with VV-Ova only. K^b-SIINFEKL-specific donor and host cells were analyzed 30 days after VV-Ova in the spleen. Plots are gated on donor or host CD8 T cells.

(B) Splenocytes from iFABP-Ova mice were transferred 30 days after 3° to naive, congenically mismatched iFABP-Ova or B6. Donor K^b-SIINFEKL$^+$ CD8 T cells were enumerated in spleen 70 days later.

(C) iFABP-Ova or B6 splenocytes were stained with K^b-SIINFEKL and K^b-N tetramers in the same sample or K^b-SIINFEKL and K^b-B8R tetramers in the same sample 30 days after 3°. Plots are gated on CD8 cells.

(D) K^b-SIINFEKL tetramer-binding CD8 T cells were tracked in the PBLs of B6 or iFABP-Ova mice following MCMV-Ova. Black solid, B6; gray dashed, iFABP-Ova.

(E) Numbers of K^b-SIINFEKL, D^b-M45, and K^b-IE3 tetramer$^+$ CD8 T cells were enumerated in the spleens of B6 or iFABP-Ova mice >140 days post-MCMV-Ova infection. M45 and IE3 are MCMV proteins. Black, B6; white, iFABP-Ova.

Representative of at least 2 experiments totaling 4–12 animals per group. ***$p < 0.0001$. Error bars indicate means ± SEMs.

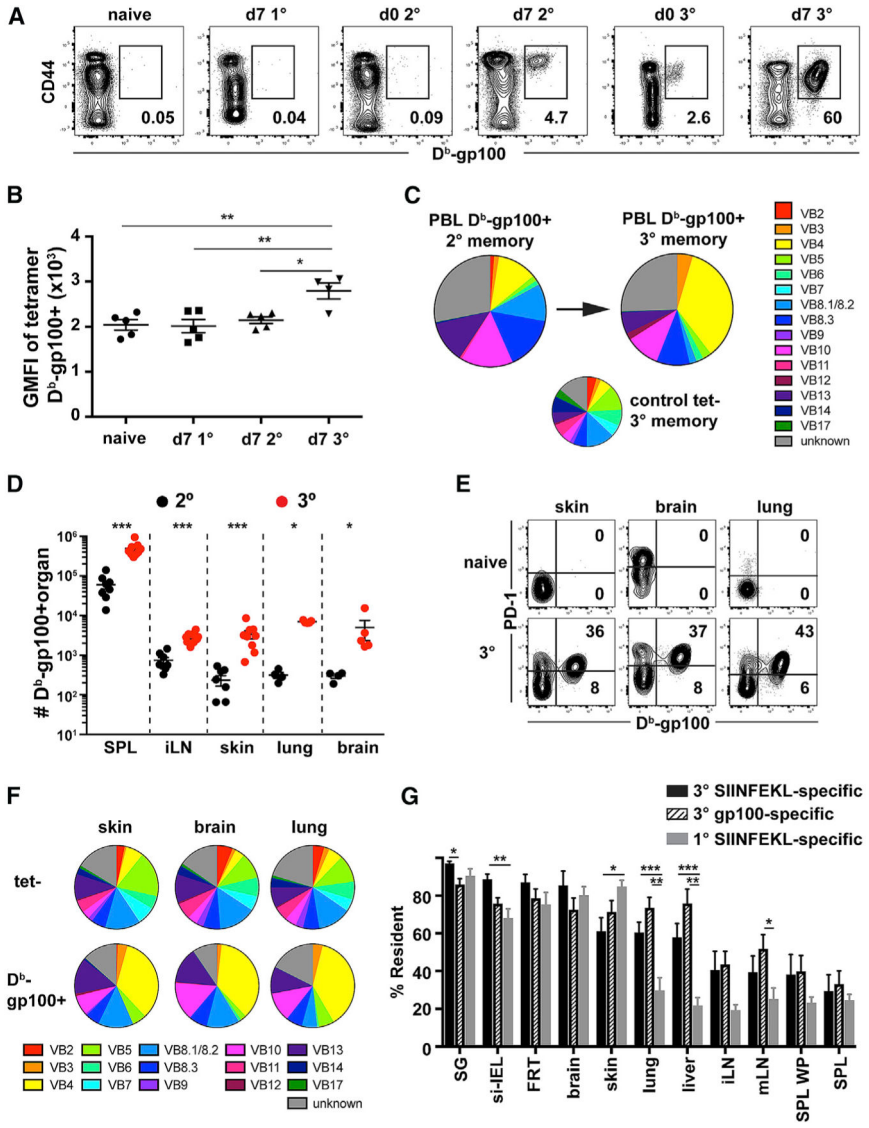

Figure 5. Sequential Immunization Breaks CD8 T Cell Tolerance to Skin-Specific Antigen and Generates Resident Memory T Cells in NLT and SLO

(A–E) B6 mice were uninfected (naive) or infected with VSV-gp100 (1°), VV-gp100 (2°), and Ad5-gp100 (3°) at least 35 days apart.

(A) PBLs were analyzed for D^b-gp100-specific CD8 T cells at indicated times. Plots are gated on CD8 T cells.

(B) GMFI of D^b-gp100 tetramer staining from animals in (A).

(C) Vβ expression after 2° and 3° in PBLs. Top: Average Vβ expression in D^b-gp100 tetramer$^+$ populations. Bottom: average Vβ expression in CD8$^+$ D^b-gp100 tetramer$^-$ population at 3°.

(D) Enumeration of D^b-gp100-specific CD8 T lymphocytes in SPL, inguinal LN (iLN), skin, lung, and brain 110 days after 2° and 89 days after 3°. Black, 2°; red, 3°.

(E) Lymphocytes from the skin, brain, and lung isolated from naive or gp100 3° immunized mice 30 days after 3°. Plots are gated on CD8 T cells.

(F) Vβ expression after 3° in skin, brain, and lung. Top: average Vβ expression in $CD8^+$ D^b-gp100 $tetramer^-$ populations. Bottom: Vβ expression in $CD8^+$ D^b-gp100 $tetramer^+$ population.

(G) Percentage residence for the indicated antigen-specific T cells. B6 mice were dual-boosted to generate both gp100- and SIINFEKL-specific CD8 T cells. Dual-boosted mice of different congenics were conjoined via parabiosis 35 days after 3°. To compare to 1° responses, B6 mice with congenically distinct memory OTI were conjoined to naive B6 mice. Black bars, 3° K^b-SIINFEKL specific; striped bars, 3° D^b-gp-100 specific; gray bars, 1° OTI memory.

All data, except PBLs, based on i.v. negative T cells. Representative of at least 2 experiments totaling 3–12 animals per group. *$p < 0.05$ and $p \geq 0.01$, **$p < 0.01$ and $p > 0.0001$, ***$p \leq 0.0001$. Error bars indicate means ± SEMs.

See also Figure S4, S5, and S6.

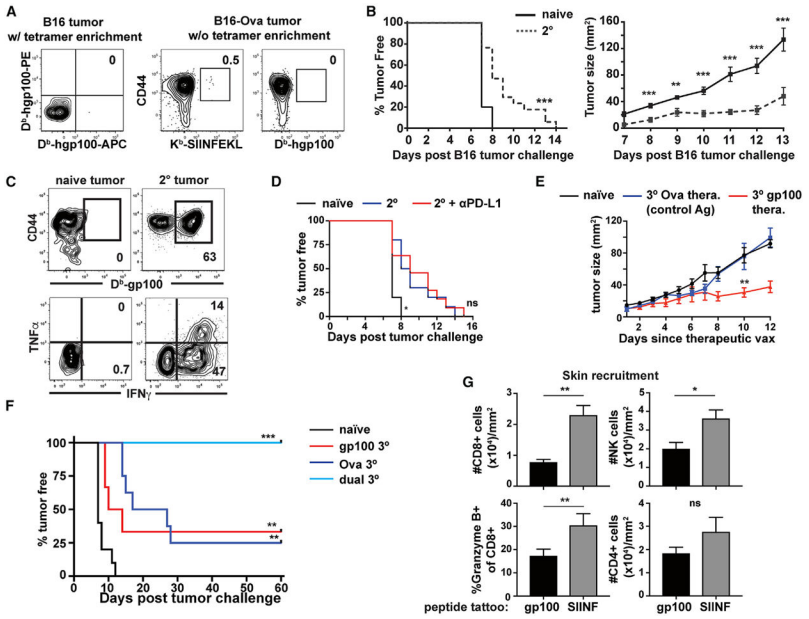

Figure 6. Self-Antigen-Specific CD8 T Cells Targeting Tumor-Associated Self-Antigen Control Melanoma Growth

(A) Visualization of antigen-specific CD8 T cells in tumors from unimmunized B6 mice. Left: frequency of D^b-gp100-specific CD8 T cells in B16 melanoma tumor isolated by tetramer enrichment 18 days after tumor challenge. Right: frequency of K^b-SIINFEKL and D^b-gp100-specific CD8 T cells in B16-Ova tumors, without tetramer enrichment 30 days after tumor challenge. Numbers in plots indicate frequency in gate.

(B and C) Mice were naive or immunized with VSV-gp100 (1°) and Ad-gp100 (2°) 35 days apart. Vaccinated and naive mice received B16 cells 2 days after 2°. Solid, naive; dashed, 2°.

(B) Percentage of tumor free (left) and tumor size (right) after challenge.

(C) Lymphocytes were isolated from tumors from naive and 2° mice in (B). D^b-gp100-specific CD8 T cells were identified by tetramer staining without enrichment (top) or 4 h *ex vivo* peptide stimulation (bottom).

(D) Mice were naive (black line) or immunized, as in (B) (blue line) ± anti-PD-L1 (red line). Graph shows percentage of tumor free after challenge.

(E) Tumor size after therapeutic vaccination with indicated vectors. B16 cells were injected into naive mice or mice ≥30 days after 2° gp100 or control 2° Ova immunizations. At day 8 after B16 injection, when mice had palpable tumors, animals either received the third gp100 boost with Ad-gp100 (red line), the third boost with Ad-Ova (blue line), or remained naive (black line).

(F) Mice were immunized with gp100 vectors, with Ova vectors, or with both concurrently. The final vaccination was given 2 days before B16-Ova challenge. Black, naive; red, gp100 only; blue, Ova only; aqua, dual-boosted. p values refer to experimental group versus naive.

(G) Recruitment of endogenous cells to the skin 48 h after tattooing skin of dual-boosted mice with SIINFEKL or gp100 peptide on opposite flanks.

Data based on i.v. negative staining T cells. Representative of experimental groups totaling 5–15 animals per group. *$p < 0.05$, **$p \leq 0.0094$, ***$p \leq 0.0008$. Error bars indicate means ± SEMs.

See also Figures S5 and S6.

KEY RESOURCE TABLE

REAGENT or RESOURCE	SOURCE	IDENTIFIER
Antibodies		
PE/Cy7 anti-CD8α antibody (53-6.7)	BioLegend	Catalog# 100722; RRID:AB_312761
Brilliant violet 605 anti-CD8α antibody (53-6.7)	BioLegend	Catalog# 100744; RRID:AB_2562609
BUV737 anti-CD8a (53-6.7)	BD Biosciences	Catalog# 564297; RRID: AB_2722580
FITC anti-CD8b (YTS156)	BioLegend	Cat# 126606; RRID: AB_961295
AF700 anti-CD4 (RM4-5)	BioLegend	Cat# 100536; RRID: AB_493701
CD4 BV711	BioLegend	Cat# 100407; RRID: AB_2564586
Alexa fluor 700 anti-CD44 antibody (IM7)	BioLegend	Catalog# 103026; RRID: AB_493713
Brilliant violet 785 anti-CD44 antibody (IM7)	BioLegend	Catalog# 103059; RRID: AB_2571953
PerCP/Cy5.5 anti-CD45.1 antibody (A20)	Tonbo	Catalog# 65-0453-U100; RRID:AB_2621893
PE anti-CD45.1 (A20)	BioLegend	Cat# 110707; RRID:AB_313496
FITC CD45.1 (A20)	Tonbo	Cat# 35-0453-4500; RRID: AB_2621691
BV711 anti-CD45.1 (A20)	BioLegend	Cat# 110739; RRID:AB_2562605
FITC anti-CD45.2 (Clone 104)	BioLegend	Cat# 109805; RRID:AB_313442
BV605 anti-CD45.2 (Clone 104)	BioLegend	Cat#10984; RRID: AB_2563485
BV605 anti-CD69 antibody (H1.2F3)	BioLegend	Cat# 10452; RRID: AB_11203710
BV421 anti-CD69 antibody (H1.2F3)	BioLegend	Cat# 104527; RRID:AB_10900250
PE/Cy7 anti-CD69 antibody (H1.2F3)	ebioscience-ThermoFisher	Catalog# 25-0691-82; RRID:AB_469637
PE-CF594 anti-CD69 antibody (H1.2F3)	BD Biosciences	Catalog# 562455; RRID:AB_11154217
efluor 450 anti-CD90.1 antibody (HIS51)	ebioscience-ThermoFisher	Catalog# 48-0900-82; RRID:AB_1272254
PE anti-CD90.1 (OX7)	BD Biosciences	Cat# 554898; RRID:AB_395589
BV510 anti-CD90.2 (30-H12)	BD Biosciences	Cat# 740103; RRID:AB_2739861
Brilliant violet 510 anti-CD103 (M290)	BD Biosciences	Catalog# 563087; RRID:AB_2721775
FITC anti-CD103 antibody (2E7)	Biolegend	Catalog# 121420; RRID:AB_10714791
PE anti-CD103 (2E7)	Biolegend	Cat# 121406; RRID:AB_1133989
PerCP/Cy5.5 anti-PD-1 (RMP1-30)	Biolegend	Catalog# 109120; RRID:AB_2566641
PE-Cy7 anti-PD1 (29F.1A12)	ThermoFisher	Cat# A14936; RRID:AB_2534374
APC anti-IFNγ (XMG1.2)	ebioscience-ThermoFisher	Catalog# 17-7311-82; RRID:AB_469504
APC anti-IFNg (XMG1.2)	BD Biosciences	Cat# 554413; RRID:AB_398551
FITC anti-IFNg (XMG1.2)	BD Biosciences	Cat# 554411; RRID:AB_395375)
APC anti-TNF (MPS-XT22)	BD Biosciences	Cat# 554420; RRID:AB_398553
PE-CF594 anti-Granzyme B (GB11)	BD Biosciences	Cat# 562462; RRID:AB_2737618
PE anti-Vb2 (B20.6)	Biolegend	Cat# 127908; RRID:AB_1227784)
BV650 anti-Vb4 (KT4)	BD Biosciences	Cat# 743022; RRID:AB_2741219
PE/Cy7 anti-Vb5 (MR9.4)	Biolegend	Cat# 139508; RRID:AB_2566021
BV711 anti-Vb6 (RR4.7)	BD Biosciences	Cat# 744594; RRID:AB_2742343)
BUV395 anti-Vb8.1/2 (MR5-2)	BD Biosciences	Cat# 744335; RRID:AB_2742163
PE anti-Vb8.3	BD Biosciences	Cat# 553664; RRID:AB_394980)
PE anti-Vb9 (MRT-2)	Biolegend	Cat# 139804; RRID:AB_10641563
BV785 anti-Vb10b (B21.5)	BD Biosciences	Cat# 742824; RRID:AB_2741076

REAGENT or RESOURCE	SOURCE	IDENTIFIER
BV605 anti-Vb11 (RR3-15)	BD Biosciences	Cat# 743678; RRID:AB_2741666
PerCPcy5.5 anti-Vb12 (MR11-1)	ThermoFisher	Cat# 46-5798-80; RRID:AB_10852552
FITC anti-Vb17 (KJ23)	BD Biosciences	Cat# 553212; RRID:AB_394710)
Anti-Gp100	Abcam	AB37078
Anti-CD4 for *in vivo* depletion (GK1.5)	BioXcell	Cat# BE0003-1; RRID:AB_1107636
Anti-CD8 for *in vivo* depletion (YTS169)	BioXcell	Cat# BE0117; RRID:AB_10950145
Anti-PD-L1 for *in vivo* blockade (10F9.G2)	BioXcell	Cat# BE0101; RRID:AB_10949073)
Bacterial and Viral Strains		
Lymphocytic choriomeningitis virus (LCMV)-Armstrong strain	Dr. R. Ahmed, Emory University	N/A
Vesicular stomatitis virus (VSV)-Ova	Dr. Leo Lefrancois, UCONN	N/A
Listeria Monocytogenes (LM)-Ova	Dr. Leo Lefrancois, UCONN	N/A
Vaccinia virus (VV)- Ova	Dr. Leo Lefrancois, UCONN	N/A
Adenovirus (Ad) 5-Ova	Dr. Thomas Griffith, U of Minnesota	N/A
Vesicular stomatitis virus (VSV)-hgp100	Dr. Kimberly Schluns, MD Anderson	N/A
Vaccinia virus (VV)-gp100	Dr. Zong Sheng Guo, U of Pittsburgh	N/A
Adenovirus (Ad)- serotype 2 gp100	Dr. Nicholas Restifo, NIH	N/A
Adenovirus (Ad)- serotype 5 gp100	Iowa Viral Vector Core	N/A
MCMV-Ova	Dr. Ann Hill, OHSU	N/A
Cell Lines		
B16 cell line	NCI-DTP	Cat# B16F10; RRID:CVCL_0159
B16-Ova	NCI-DTP	RRID:CVCL_WM77
Chemicals, Peptides, and Recombinant Proteins		
SIINFEKL	New England Peptide	N/A
EGSRNQDWL	New England Peptide	N/A
KVPRNQDWL	New England Peptide	N/A
DL-Dithioerythritol (DTE)	VWR Scientific	Catalog# 97061-642
Collagenase I	Worthington Biochemicals	Catalog# LS004197
Collagenase III	Worthington Biochemicals	Catalog# LS004183
CFSE	BD Biosciences	Cat# 565082
4',6-Diamidino-2-Phenylindole dihydrochloride (DAPI)	Sigma Aldrich	Catalog# D9542
Live dead Ghost Dye Red 780	Tonbo Biosciences	Catalog# 13-0865-T500
H-2Db/GP_{33-41} KAVYNFATM biotinylated monomer	Prepared in house following NIAID tetramer core facility protocol	N/A
H-2Kb /$OVA_{257-264}$ SIINFEKL biotinylated monomer	Prepared in house following NIAID tetramer core facility protocol	N/A
H-2Kb/B8R RGYVYQGL biotinylated monomer	Prepared in house following NIAID tetramer core facility protocol	N/A
H-2Kb/N TSYKFESV biotinylated monomer	Prepared in house following NIAID tetramer core facility protocol	N/A
H-2Db/M45 HGIRNASFI biotinylated monomer	Prepared in house following NIAID tetramer core facility protocol	N/A

REAGENT or RESOURCE	SOURCE	IDENTIFIER
H-2Kb/IE3 RALEYKNL biotinylated monomer	Prepared in house following NIAID tetramer core facility protocol	N/A
I-A^b/LM $LLO_{190-201}$ tetramer	Dr. Marc Jenkins, U of Minnesota	N/A
H2-Db/ mgp100 EGSRNQDWL biotinylated monomer	Prepared in house following NIAID tetramer core facility protocol	N/A
H2-Db/ hgp100 KVPRNQDW biotinylated monomer	Prepared in house following NIAID tetramer core facility protocol	N/A
Streptavidin-APC (monomer tetramerization)	Life Technologies	Catalog# S868
Streptavidin-PE (monomer tetramerization)	Life Technologies	Catalog# S866
Critical Commercial Assays		
iFABP- ELISA	Elabscience	E-EL-M0735
Experimental Models: Organisms/Strains		
C57BL/6J	The Jackson Laboratory	Catalog# JAX:000664; RRID: IMSR_JAX: 000664
iFABP-OVA CD45.2 or CD45.1	Dr. Leo Lefrancois, UCONN	N/A
P14	Dr. R. Ahmed, Emory University	Catalog# MUGEN:M189001; RRID: IMSR_MUGEN:M189001
OT-I 45.1	Dr. K. Hogquist, Univ. of Minnesota	Catalog# JAX:003831; RRID: IMSR_JAX: 003831
OT-I Thy1.1	Dr. K. Hogquist, Univ. of Minnesota	N/A
B6 CD45.1	Bred in house	N/A
B6 Thy1.1	The Jackson Laboratory	Catalog# JAX:000406; RRID: IMSR_JAX: 000406
Software and Algorithms		
Flowjo v9 and v10	Treestar Inc	RRID:SCR_008520
Prism 7	Graphpad Inc	RRID:SCR_002798
Image J4	NIH	N/A